ARTICLE

Equivalence and its invalidation between non-Markovian and Markovian spreading dynamics on complex networks

Mi Feng [1,2,3], Shi-Min Cai[2,3], Ming Tang [1,4] & Ying-Cheng Lai [5]

Epidemic spreading processes in the real world depend on human behaviors and, consequently, are typically non-Markovian in that the key events underlying the spreading dynamics cannot be described as a Poisson random process and the corresponding event time is not exponentially distributed. In contrast to Markovian type of spreading dynamics for which mathematical theories have been well developed, we lack a comprehensive framework to analyze and fully understand non-Markovian spreading processes. Here we develop a mean-field theory to address this challenge, and demonstrate that the theory enables accurate prediction of both the transient phase and the steady states of non-Markovian susceptible-infected-susceptible spreading dynamics on synthetic and empirical networks. We further find that the existence of equivalence between non-Markovian and Markovian spreading depends on a specific edge activation mechanism. In particular, when temporal correlations are absent on active edges, the equivalence can be expected; otherwise, an exact equivalence no longer holds.

[1] School of Mathematical Sciences, Shanghai Key Laboratory of PMMP, East China Normal University, Shanghai 200241, China. [2] Web Sciences Center, University of Electronic Science and Technology of China, Chengdu 611731, China. [3] Big Data Research Center, University of Electronic Science and Technology of China, Chengdu 611731, China. [4] Shanghai Key Laboratory of Multidimensional Information Processing, East China Normal University, Shanghai 200241, China. [5] School of Electrical, Computer and Energy Engineering, Arizona State University, Tempe, AZ 85287, USA. Correspondence and requests for materials should be addressed to M.T. (email: tangminghan007@gmail.com)

Disease or virus spreading on complex networks, because of its broad relevance to health care, social, economical, and political sciences as well as information technologies, has been an active area of research on contemporary network science and engineering[1–8]. Traditional models of spreading dynamics on networks are memoryless Markovian in the sense that, for all individuals in the network, both contracting a virus and recovering from it are viewed as a Poisson process. The time interval between two successive contracting events and that between two adjacent recovery events follow an exponential distribution with a constant rate—the arrival rate of the respective Poisson process. Associated with the exponential distribution is the memoryless property: any future waiting time does not depend on the previous waiting time. This property fits with that of a memoryless Markovian process as, what matters in order to predict the future is the current state, not the history of the process. The Markovian assumption greatly facilitates the development of mathematical theories of spreading process on complex networks[5,7] through, e.g., a mean-field type of analyses[1,9–11] of the standard susceptible-infected-susceptible (SIS) or susceptible-infected-recovered (SIR) process. There has been increasing empirical evidence and modeling effort that the occurrences of contacts associated with human activities are non-Markovian temporal processes with a heavy tailed inter-event time distribution[12–33]. A Markovian description of network spreading dynamics is thus ideal and provides only an approximate picture of the real world.

The past decade has witnessed a growing interest in non-Markovian spreading dynamics on complex networks[34–50]. The failure of the Markovian framework in describing human interactions in relation to disease spreading was noted quite early, and it was found that the deviation from the exponential distribution of the inter-event time to being heterogeneous can impede spreading[35]. A non-Markovian SIR model with arbitrary time distributions of infection and recovery was solved through the approach of dynamical message passing[37]. It was also found that a heavy-tailed waiting time distribution can slow down the prevalence decay[39]. An SIR model with fixed recovery time but with a heavy-tailed infection time distribution was studied with the finding that temporal heterogeneity in the contact process can significantly suppress epidemic spreading[40]. A relatively significant alteration of the outbreak threshold was reported for non-Markovian type of SIS infection events and certain equivalence between non-Markovian and Markovian models through redefining the effective infection rate was pointed out[41,42]. Two basic dynamical rules governing a non-Markovian type of SIS spreading process were uncovered[43]. More recently, a method was proposed to estimate the effective infection rate for non-Markovian type of spreading dynamics[47].

A common theoretical tool to deal with network spreading dynamics is mean-field analysis. The earlier version of the mean-field theory assumed that all nodes in the network are regarded as statistically equivalent[9]. To account for the non-homogeneous nature of real world networks, a heterogeneous mean field theory was developed in which the nodes with the same degree are considered as equivalent[1]. A more systematic approach to fully capturing the network topology was articulated—the so-called quench mean-field approximation[10,11]. To take into account dynamic correlations, the method of pairwise approximation can be exploited[51–54] which centers about analyzing the evolution of the states of nodal pairs. An approximate master equation theory can lead to more accurate theoretical predictions and can be reduced to the pair-wise approximation theory and the mean field theory through proper approximations[55]. A mean-field analysis based on the pair approximation for non-Markovian SIR dynamics on networks was recently developed[45,46,48].

Our work is motivated by two considerations. The first concerns about the development of a general theoretical framework to deal with non-Markovian processes. In particular, in spite of the previous studies, a comprehensive framework to analyze and understand the full dynamical evolution of non-Markovian spreading processes is still lacking. Especially, in the existing literature on network spreading dynamics, Markovian or non-Markovian, a central focus has been on the final steady state of the system, with the transient dynamics leading to the final state largely ignored. In nonlinear dynamical systems, transient behaviors have been recognized as relevant as or even more important than the final state. For example, transient chaos arises commonly in nonlinear dynamical systems and is typically more ubiquitous than attractors (final states)[56]. In ecological systems, transient dynamics have been long recognized as the main source on which empirical observations rely and are thus a key driving force of natural evolution[57–61]. For non-Markovian type of network spreading dynamics, we lack a theory to describe both transient dynamics and final steady state. The second motivation is that, since Markovian spreading processes, while ideal, are amenable to rigorous mathematical analyses and thus often afford a complete understanding of the detailed underlying dynamics, it is of great interest to uncover conditions under which a non-Markovian process is equivalent to or can be approximated by a Markovian one.

In this paper, we articulate a first-order mean field theory for SIS dynamics with non-Markovian infection and recovery processes. We define the probability density function of state age of node (or of edge) and derive the corresponding partial differential equations that govern the evolution of the density functions. We demonstrate that the theory can predict well both the transient behaviors and the steady states of non-Markovian spreading on synthetic and empirical networks. A key finding is that the edge activation rule determines whether there is an equivalence between non-Markovian and Markovian SIS dynamics, and we show that a specific type of activation rule can lead to an exact equivalence. For non-Markovian processes that are not equivalent to Markovian ones, a relatively large infection density of the whole network makes the process closer to being Markovian. With the ability to analyze transient dynamics, the developed theoretical framework not only leads to a picture of the entire evolution process of non-Markovian spreading dynamics, but also results in a deeper understanding of the conditions under which a non-Markovian process is equivalent to a Markovian one.

Results

Non-Markovian spreading dynamics on complex networks. In the classical, Markovian SIS model, a node in a network can be in the susceptible or infected state. An infected node can pass on the virus to any of its susceptible neighbors at certain transmission rate and return to the pool of susceptible nodes at a fixed recovery rate. Because of the Markovian and memoryless nature of the model, transmission of disease and recovery of nodes both are Poisson processes, i.e., both the infection and recovery time are exponentially distributed. In contrast, in a non-Markovian epidemic process with memory, neither the infection nor the recovery time follows an exponential distribution. Instead, such distributions are typically "fat-tailed" due to the highly heterogeneous nature of various human behaviors[12–33].

For a non-Markovian epidemic process, the infection and recovery rates are generally time dependent. To gain insights into defining these rates, we begin with a key quantity: the infection age (or susceptibility age) τ of a node, which is the time elapsed from the birth of its current state, i.e., an infected state or a

susceptible state, to the current time t. If a node becomes infected at time $t - \tau$ and has not recovered by time t, its infection age at time t will be τ. An infected node decays spontaneously into the susceptible state after a random time τ whose probability distribution is $\psi_{rec}(\tau)$, indicating that the infected node will recover during the infinitesimal infection age interval $(\tau, \tau + d\tau)$ with the probability $\psi_{rec}(\tau)d\tau$. Similarly, the activation age (or non-activation age) κ of an edge can be defined, where the active edges host statistically independent stochastic infection processes of the same distribution $\psi_{inf}(\kappa)$. That is, the probability that an active edge transmits the disease during the infinitesimal active age interval $(\kappa, \kappa + d\kappa)$ is $\psi_{inf}(\kappa)d\kappa$. If a susceptible node has more than one active edge, an infection process will take place independently along each active edge.

The time dependent recovery and infection rates can then be evaluated[43,47] based on the distributions $\psi_{rec}(\tau)$ and $\psi_{inf}(\kappa)$. In particular, if an event has not taken place by a time since the process was initiated, it will take place in the next time interval with a conditional probability. The recovery and infection rates are thus given by, respectively,

$$\omega_{rec}(\tau) = \frac{\psi_{rec}(\tau)}{\Psi_{rec}(\tau)} \qquad (1)$$

and

$$\omega_{inf}(\kappa) = \frac{\psi_{inf}(\kappa)}{\Psi_{inf}(\kappa)}, \qquad (2)$$

where $\Psi_{rec}(\tau)$ and $\Psi_{inf}(\kappa)$ are the corresponding survival probabilities. Especially,

$$\Psi_{rec}(\tau) = \int_{\tau}^{+\infty} \psi_{rec}(\tau')d\tau' \qquad (3)$$

is the probability that the infected node will not recover before the infection age τ and

$$\Psi_{inf}(\kappa) = \int_{\kappa}^{+\infty} \psi_{inf}(\kappa')d\kappa' \qquad (4)$$

is the probability that the active edge never transmits the disease in the range of the active age from 0 to κ. Substituting $\Psi_{rec}(\tau)$ and $\Psi_{inf}(\kappa)$ into Eqs. (1) and (2), we obtain

$$\Psi_{rec}(\tau) = e^{-\int_0^{\tau} \omega_{rec}(\tau')d\tau'} \qquad (5)$$

and

$$\Psi_{inf}(\kappa) = e^{-\int_0^{\kappa} \omega_{inf}(\kappa')d\kappa'} \qquad (6)$$

The recovery and infection time distributions can thus be expressed, respectively, as

$$\psi_{rec}(\tau) = \omega_{rec}(\tau)e^{-\int_0^{\tau} \omega_{rec}(\tau')d\tau'}, \qquad (7)$$

and

$$\psi_{inf}(\kappa) = \omega_{inf}(\kappa)e^{-\int_0^{\kappa} \omega_{inf}(\kappa')d\kappa'}. \qquad (8)$$

In the special case of memoryless Markovian model, the temporal processes follow the Poisson statistics, where the distributions are exponential with their respective constant rate.

For epidemic spreading on a network, there are various mechanisms to activate edges. We focus on the two basic mechanisms to generate active edges[43,47]. In general, an undirected edge can be regarded as being equivalent to two directed edges in the opposite directions, and a directed edge with starting node j and ending node i is denoted as $i \leftarrow j$. For the first mechanism (type-I), which is the same as rule 1 in ref. [43], one defines a directed link $i \leftarrow j$ as an active edge when node j is an infected node and node i is susceptible. If an active edge $i \leftarrow j$

transmits the disease, the healthy node i will turn into the infected state and the edge $i \leftarrow j$ will become non-active. For the second mechanism (type-II), which is the same as that in ref. [47], a directed link $i \leftarrow j$ is defined as an active edge when node j is an infected node regardless of the state of node i. Once the active edge $i \leftarrow j$ transmits the disease, node i will turn into the infected state if it is susceptible, or nothing happens to node i if it is already infected. At the same time, the active edge $i \leftarrow j$ will become a new active edge with active age $\kappa = 0$. Figure 1 shows the cases in which the active age of an active edge is zero. In the special case of non-Markovian process where $\psi_{inf}(\kappa)$ follows an exponential distribution and the infection rate $\omega_{inf}(\kappa)$ is a constant independent of time, the SIS models constructed according to the two respective mechanisms are equivalent.

First-order mean-field theory for non-Markovian spreading. To describe the full dynamical evolution of non-Markovian epidemic spreading on networks, we articulate a theoretical framework based on the approach of first-order mean-field analysis. Specifically, we begin by defining $I_i(\tau; t)$ and $S_i(\tau; t)$ as the probability density functions that node i stays in the infected and susceptible state aged τ at time t, respectively[48]. The probability of node i being in the infected state aged from τ to $\tau + d\tau$ is thus $I_i(\tau; t)d\tau$. In the time interval $(t, t + dt)$, node i returns to the susceptible state with probability $\omega_{rec}(\tau)dt$ and the probability that the state of the node remains unchanged is $1 - \omega_{rec}(\tau)dt$. After the infinitesimal time interval dt has elapsed, the age of node i and that of the active edge $i \leftarrow j$ both will increase by the amount dt. We thus have $dt = d\tau = d\kappa$. At time $t + dt$, the probability density function that node i still remains in the infected state aged $\tau + d\tau$ is given by

$$I_i(\tau + d\tau; t + dt) = [1 - \omega_{rec}(\tau)d\tau]I_i(\tau; t). \qquad (9)$$

This difference equation can be rewritten as a partial differential equation:

$$\left(\frac{\partial}{\partial \tau} + \frac{\partial}{\partial t}\right)I_i(\tau; t) = -\omega_{rec}(\tau)I_i(\tau; t). \qquad (10)$$

Since the infected node i with infection age ranging from 0 to $+\infty$ can switch into the susceptible state of age zero insofar as there is a recovery, the probability density function that node i returns to the susceptible state aged $\tau = 0$ is

$$S_i(0; t + dt) = \int_0^{+\infty} \omega_{rec}(\tau)I_i(\tau; t)d\tau. \qquad (11)$$

To describe the time evolution of $S_i(\tau; t)$, we assume that the ages of two connected nodes are uncorrelated. The probability density function that node i in the susceptible state of age τ is infected by node j at time t can be written as $\Phi_{i \leftarrow j}(\tau; t)$. During the time interval $(t, t + dt)$, the susceptible node i aged τ is infected by its neighbors with the probability $\sum_{j=1}^{N} a_{ij}\Phi_{i \leftarrow j}(\tau; t)d\tau$, where N is the network size and a_{ij} is the ijth element of the network adjacency matrix. We thus get the partial differential equation governing the evolution of $S_i(\tau; t)$ as

$$\left(\frac{\partial}{\partial \tau} + \frac{\partial}{\partial t}\right)S_i(\tau; t) = -S_i(\tau; t)\sum_{j=1}^{N} a_{ij}\Phi_{i \leftarrow j}(\tau; t). \qquad (12)$$

Since a susceptible node i with any susceptibility age ranging from 0 to $+\infty$ can be infected and switches into the infected state aged zero as a result of the infection process, the probability density
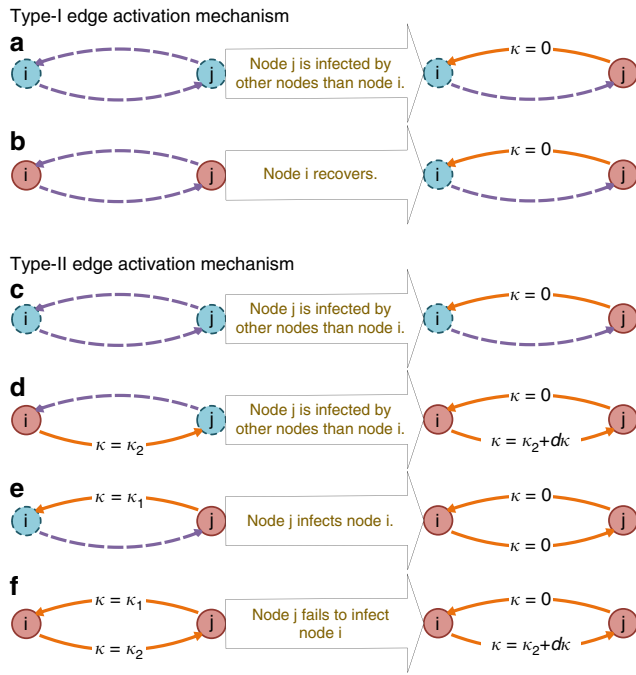
Fig. 1 Two mechanisms to activate edges. For the first mechanism (type-I), there are two cases in which the state age of an active edge is set to zero: **a** the event is driven by the generation of infected node, **b** it results from the generation of an susceptible node. For the second mechanism (type-II), there are four independent scenarios for setting zero the age of an active edge: **c**, **d** the event occurs because of the generation of an infected node, **e**, **f** it is caused by the transmission of the disease. Blue dashed and red solid circles represent susceptible and infected nodes, respectively. Purple dashed and orange solid arrows denote nonactive and active edges, respectively. Each state transition takes place in an infinitesimal time interval $d\tau$ or $d\kappa$, where $d\tau = d\kappa$

function that node i enters into the infected state aged $\tau = 0$ is

$$I_i(0; t + dt) = \int_0^{+\infty} S_i(\tau; t) \sum_{j=1}^N a_{ij} \Phi_{i \leftarrow j}(\tau; t) d\tau. \tag{13}$$

For different activation mechanisms of active edges, namely, type-I and type-II, the forms of $\Phi_{i \leftarrow j}(\tau; t)$ are different. For type-I mechanism, once an infected node j and a susceptible node i appear on both ends of an edge, the directed edge $i \leftarrow j$ will be activated or, equivalently, the edge will enter into an active state aged $\kappa = 0$. Ignoring the dynamical correlation between any pairwise nodes, the age of the active edge is determined by the smaller age of the connected nodes, $\min(\tau, \tau')$, where τ and τ' are the susceptibility age of node i and the infection age of node j, respectively. We thus have

$$\Phi_{i \leftarrow j}(\tau; t) = \int_0^{+\infty} \omega_{\text{inf}}[\min(\tau, \tau')] I_j(\tau'; t) d\tau', \tag{14}$$

where $\omega_{\text{inf}}[\min(\tau, \tau')]$ is the infection rate of the active edge whose age is equal to the smaller one of the end nodes.

For type-II mechanism, the age of the active edge $i \leftarrow j$ depends on the infected node j only, and we have

$$\Phi_{i \leftarrow j}(\tau; t) = \int_0^{+\infty} \eta(\tau') I_j(\tau'; t) d\tau', \tag{15}$$

where the infection rate $\eta(\tau)$ of the infected node j aged τ satisfies

the integral equation

$$\eta(\tau) = \int_0^\tau \eta(\tau') \psi_{\text{inf}}(\tau - \tau') d\tau' + \psi_{\text{inf}}(\tau). \tag{16}$$

The solution of Eq. (16) can be written as

$$\eta(\tau) = \int_{\sigma - i\infty}^{\sigma + i\infty} \frac{\hat{\psi}_{\text{inf}}(s)}{1 - \hat{\psi}_{\text{inf}}(s)} e^{s\tau} ds, \tag{17}$$

where $\hat{\psi}_{\text{inf}}(s)$ is the Laplace transform of $\psi_{\text{inf}}(\tau)$:

$$\hat{\psi}_{\text{inf}}(s) = \int_0^{+\infty} \psi_{\text{inf}}(\tau) e^{-s\tau} d\tau \tag{18}$$

Supplementary Fig. 1 in Supplementary Note 2 presents the analysis of $\eta(\tau)$ for type-II edge activation mechanism.

Equations (10) and (12) govern the time evolution of non-Markovian SIS spreading dynamics in general, with the boundary conditions given by Eqs. (11) and (13). The state transition processes can be described as the probability flows between the infected and susceptible states determined by the functions $I_i(\tau; t)$ and $S_i(\tau; t)$, as well as those within each state. A schematic illustration of the various probability flows is shown in Fig. 2. The initial conditions for Eqs. (10) and (12) are the initial probability distributions of each node:

$$I_i(\tau; 0) = \rho_i(\tau) \tag{19}$$

and

$$S_i(\tau; 0) = \chi_i(\tau), \tag{20}$$

where $\rho_i(\tau)$ and $\chi_i(\tau)$ are the probability densities of the ages of node i being in the infected and susceptible state, respectively.

Transient behaviors. To test the power of our mean-field theory to predict transient behaviors in non-Markovian processes, we carry out Monte Carlo simulations[47,62] of SIS dynamics on different types of networks (see "Methods" for details). To be general, in the simulations, we set $\psi_{\text{inf}}(\kappa)$ and $\psi_{\text{rec}}(\tau)$ to be the long-tailed, Weibull type of distribution as

$$\psi_{\text{inf}}(\kappa) = \frac{\alpha_{\text{I}}}{\beta_{\text{I}}} \left(\frac{\kappa}{\beta_{\text{I}}}\right)^{\alpha_{\text{I}} - 1} e^{-\left(\frac{\kappa}{\beta_{\text{I}}}\right)^{\alpha_{\text{I}}}} \tag{21}$$

and

$$\psi_{\text{rec}}(\tau) = \frac{\alpha_{\text{R}}}{\beta_{\text{R}}} \left(\frac{\tau}{\beta_{\text{R}}}\right)^{\alpha_{\text{R}} - 1} e^{-\left(\frac{\tau}{\beta_{\text{R}}}\right)^{\alpha_{\text{R}}}}, \tag{22}$$

where $(\alpha_{\text{I}}, \alpha_{\text{R}})$ are the shape parameters and $(\beta_{\text{I}}, \beta_{\text{R}})$ are scale parameters. A smaller value of the shape parameter and/or a larger value of the scale parameter corresponds to more extensive heterogeneity of the age distribution.

Figure 3 shows, for three different types of networks, the evolution of the infected density of the entire network over time, where the density value predicted by the mean-field theory is calculated with $I(t) = \sum_{i=1}^N I_i(t)/N$. Initially, 1% of the nodes are randomly chosen to be the infection seed and their infection ages are all zero. A small α_{I} value for which the distribution $\psi_{\text{inf}}(\kappa)$ is strongly heterogeneous will lead to a large-scale disease outbreak, due mainly to the small mean infection time. In Fig. 3a–c, the Monte-Carlo simulation results and the theoretical predictions for the type-I activation mechanism are presented for Erdös-Rényi (ER) random, Barabási-Albert (BA) scale-free, and Hamsterster networks, respectively. The Hamsterster network is a real-world social network in the human society[63]. Figure 3d–f shows the comparison results of the temporal evolution of the infected density for processes with type-II activation mechanism. The mean-field predictions of the time evolution are generally in good agreement with those of non-Markovian type of SIS
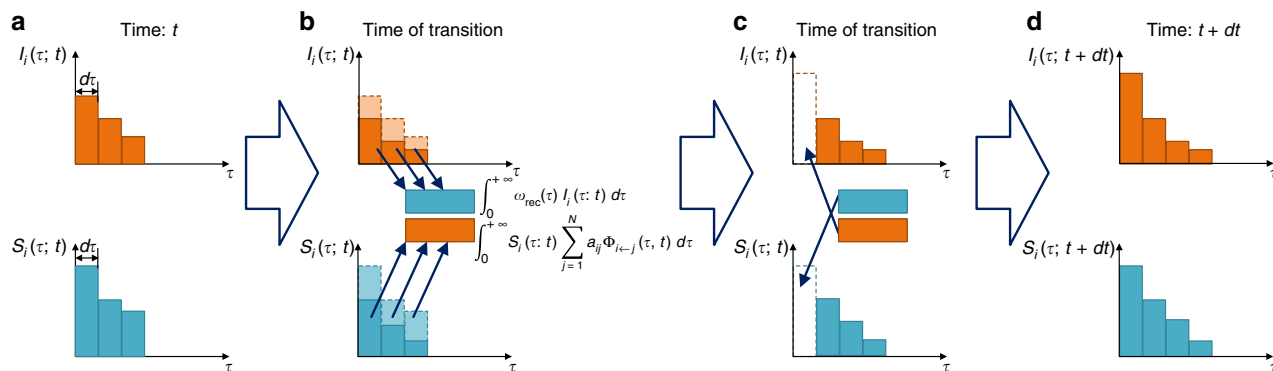
Fig. 2 Schematic representation of probability flows. Each illustration is divided into blocks of width $d\tau \to 0$, and the area of each block represents the probability that node i is in the corresponding state aged from τ to $\tau + d\tau$. **a** Two distributions, $I_i(\tau; t)$ and $S_i(\tau; t)$, of node i at time t. **b** Each block losses probability $\omega_{rec}(\tau)I_i(\tau; t)d\tau$ or $S_i(\tau; t)\sum_{j=1}^{N} a_{ij}\Phi_{i\leftarrow j}(\tau; t)d\tau$ and converges to $\int_0^{+\infty} \omega_{rec}(\tau)I_i(\tau; t)d\tau$ and $\int_0^{+\infty} S_i(\tau; t)\sum_{j=1}^{N} a_{ij}\Phi_{i\leftarrow j}(\tau; t)d\tau$, respectively. **c** Each block moves one step to the right, and the empty blocks $S_i(0; t+dt)$ and $I_i(0; t+dt)$ are filled with the probabilities $\int_0^{+\infty} \omega_{rec}(\tau)I_i(\tau; t)d\tau$ and $\int_0^{+\infty} S_i(\tau; t)\sum_{j=1}^{N} a_{ij}\Phi_{i\leftarrow j}(\tau; t)d\tau$, respectively. **d** The distributions $I_i(\tau; t+dt)$ and $S_i(\tau; t+dt)$ at time $t+dt$
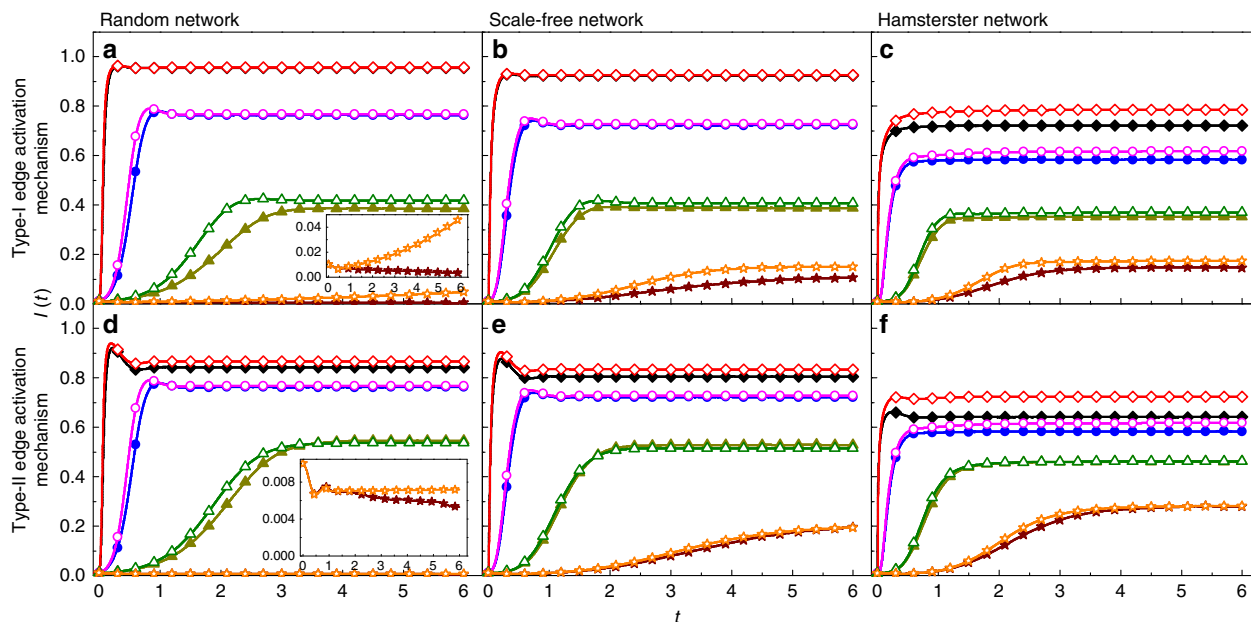
Fig. 3 (Color online) Comparison of time evolution between simulated and theoretical results. Panels in the first and second rows (**a**–**c** and **d**–**f**), respectively, are for the type-I and type-II mechanisms. The three columns from left to right are for ER random, BA scale-free, and Hamsterster networks, respectively. In all panels, the solid symbols represent the results of simulations which are averaged over 100 realizations for random and scale-free networks, and over 400 realizations for the Hamsterster network. The open symbols represent the results of theoretical solutions obtained from Eqs. (10)–(13). The symbols diamonds, circles, triangles, and stars correspond to $\alpha_I = 0.5, 1, 2, 4$, respectively. The random and scale-free networks have size $N = 10^4$ and mean degree $\langle k \rangle \approx 10$, and the Hamsterster network has $N = 2426$ and $\langle k \rangle \approx 13.7$. The insets in panels **a**, **d** show the extinction process with $\alpha_I = 4$. Other parameters are $\beta_I = 1$, $\alpha_R = 2$, and $\beta_R = 0.5$

spreading dynamics on random (homogeneous), scale-free (heterogeneous), and Hamsterster (real-world) networks.

However, in some cases (e.g., $\alpha_I = 4$ for ER random networks), there are some discrepancies between the predictions from the first-order mean-field theory and the simulation results [c.f., insets in Fig. 3a, d], due to the exclusion of any dynamical correlation. For a more accurate description of non-Markovian spreading processes, the dynamical correlation in the evolution of states of connected nodal pairs must be taken into account. To

meet this challenge, we articulate a second-order mean field approach and show that it is capable of predicting the simulation results more accurately than the first-order theory, even for extreme situations where the disease decays rapidly [e.g., the $\alpha_I = 4$ case in Supplementary Fig. 2c, d]. The second-order theory indicates that, in general, dynamical correlation such as temporal correlation between active edges can significantly affect the accuracy of the mean-field analysis (see Supplementary Fig. 2 and Supplementary Note 3 for details). Due to the limitation of

computational feasibility, we have tested the predictions of the second-order mean field theory for homogeneous networks. To extend the study to heterogeneous networks is currently infeasible due to the extreme high computational complexity required to treat all possible nodal pairs separately.

We further investigate the effects of infection time distribution and degree distribution on the transient time in Supplementary Notes 4 and 5, respectively. For a certain network topology and a given edge activation mechanism, a larger value of the shape parameter α_I leads to a longer transient phase. Intuitively, a narrower distribution of the infecting activities makes it easier for the system to reach a final steady state. (Supplementary Fig. 3 displays results on transient time versus α_I). For fixed values of the structural and dynamical parameters, random networks lead to longer transients, due mainly to the lack of hub nodes that can act as "super-spreaders". We find that a smaller value of the power-law exponent and a larger value of the lower-cutoff degree can lead to a shorter transient lifetime, indicating that hub nodes in a scale-free network can expedite spreading processes of the non-Markovian type. Supplementary Fig. 4 presents systematic results on the transient lifetime versus the values of the power-law exponent and the lower-cutoff degree.

Equivalence between non-Markovian and Markovian spreading. To establish the conditions under which an equivalence between non-Markovian and Markovian type of SIS spreading dynamics arises, we analyze the steady-state behavior. For non-Markovian type of SIS spreading dynamics for $t \to +\infty$, we define the following asymptotic probability density functions:

$$\tilde{I}_i(\tau) = \lim_{t \to +\infty} I_i(\tau; t), \tag{23}$$

$$\tilde{S}_i(\tau) = \lim_{t \to +\infty} S_i(\tau; t), \tag{24}$$

$$\tilde{\Phi}_{i \leftarrow j}(\tau) = \lim_{t \to +\infty} \Phi_{i \leftarrow j}(\tau; t). \tag{25}$$

From Eqs. (10) and (12), we obtain the differential equations for the probability density functions in the steady state as

$$\frac{d\tilde{I}_i(\tau)}{d\tau} = -\omega_{\text{rec}}(\tau)\tilde{I}_i(\tau), \tag{26}$$

$$\frac{d\tilde{S}_i(\tau)}{d\tau} = -\tilde{S}_i(\tau) \sum_{j=1}^{N} a_{ij} \tilde{\Phi}_{i \leftarrow j}(\tau). \tag{27}$$

In the steady state, the probabilities that a node is newly infected and that a node recovers are equal[11], so we have

$$\tilde{I}_i(0) = \tilde{S}_i(0). \tag{28}$$

In the steady state, the probabilities that node i is in the infected state and in the susceptible state are, respectively,

$$\tilde{I}_i = \int_0^{+\infty} \tilde{I}_i(\tau) d\tau \tag{29}$$

and

$$\tilde{S}_i = \int_0^{+\infty} \tilde{S}_i(\tau) d\tau. \tag{30}$$

For type-I activation mechanism, we can obtain a relation between the probabilities of node i being in the infected and susceptible state as

$$\frac{1}{\tilde{I}_i} = \frac{1}{\tilde{S}_i} \sum_{n=1}^{+\infty} \delta_{\text{eff}} \vartheta^{(n)}(0) \left(\frac{1}{\sum_{j=1}^{N} a_{ij} \tilde{I}_j} \right)^n, \tag{31}$$

or

$$\frac{1}{\tilde{I}_i} = \frac{1}{\lambda_{\text{eff}}^* \tilde{S}_i \sum_{j=1}^{N} a_{ij} \tilde{I}_j} + \frac{1}{\tilde{S}_i} \sum_{n=2}^{+\infty} \delta_{\text{eff}} \vartheta^{(n)}(0) \left(\frac{1}{\sum_{j=1}^{N} a_{ij} \tilde{I}_j} \right)^n, \tag{32}$$

where the effective recovery rate is

$$\delta_{\text{eff}} = \frac{1}{\int_0^{+\infty} \Psi_{\text{rec}}(\tau) d\tau}, \tag{33}$$

$\vartheta(\tau)$ is the inverse of the function $\Omega(\tau)$ given by

$$\Omega(\tau) = \delta_{\text{eff}} \int_0^{\tau} \int_0^{+\infty} \omega_{\text{inf}}[\min(\tau', \tau'')] \Psi_{\text{rec}}(\tau') d\tau' d\tau'', \tag{34}$$

and $\vartheta^{(n)}(0)$ is the nth derivative of $\vartheta(\tau)$ at $\tau = 0$ and λ_{eff}^* is defined as

$$\lambda_{\text{eff}}^* = 1/[\delta_{\text{eff}} \vartheta^{(1)}(0)]. \tag{35}$$

The procedure to derive Eqs. (31) and (32) is detailed in Supplementary Note 1.

For type-II activation mechanism, the relation between the probabilities can be obtained as

$$\tilde{I}_i = \lambda_{\text{eff}} \tilde{S}_i \sum_{j=1}^{N} a_{ij} \tilde{I}_j, \tag{36}$$

where λ_{eff} is the effective infection rate with the specific form

$$\lambda_{\text{eff}} = \int_0^{+\infty} \eta(\tau) \Psi_{\text{rec}}(\tau) d\tau. \tag{37}$$

Substituting Eq. (17) for $\eta(\tau)$ into Eq. (37), we have

$$\lambda_{\text{eff}} = \frac{1}{2\pi i} \int_C \frac{\hat{\psi}_{\text{inf}}(s) \hat{\psi}_{\text{rec}}(-s)}{1 - \hat{\psi}_{\text{inf}}(s)} \frac{ds}{s}, \tag{38}$$

where $\hat{\psi}_{\text{inf}}(s) = \int_0^{+\infty} \psi_{\text{inf}}(\tau) e^{-s\tau} d\tau$, $\hat{\psi}_{\text{rec}}(s) = \int_0^{+\infty} \psi_{\text{rec}}(\tau) e^{-s\tau} d\tau$, and C is a contour that encloses the entire $\text{Re}(s) > 0$ region[42,64] (see Supplementary Note 2 for details).

Under what conditions can one expect the non-Markovian SIS dynamics to reduce to Markovian dynamics in the steady state? To address this question, we note that the equivalence requires that the non-Markovian steady-state equations be written[42,47] in the form of Eq. (36), or

$$\frac{1}{\tilde{I}_i} = \frac{1}{\lambda_{\text{eff}} \tilde{S}_i \sum_{j=1}^{N} a_{ij} \tilde{I}_j}. \tag{39}$$

For non-Markovian SIS spreading dynamics with type-II activation mechanism, such an equivalence does exist.

However, for processes with type-I activation mechanism, because of the high-order terms ($n \geq 2$) in Eq. (32), in general an equivalence to Markovian dynamics cannot be expected. Nonetheless, under certain conditions, an approximate equivalence can arise. In particular, if both $\vartheta^{(1)}(0)$ and $\vartheta^{(n)}(0)(n \geq 2)$ have a finite value, a large value of $\sum_{j=1}^{N} a_{ij} \tilde{I}_j$ will dominate the right-hand side of Eq. (32), making the high-order terms $\sum_{n=2}^{+\infty} \vartheta^{(n)}(0)(1/\sum_{j=1}^{N} a_{ij} \tilde{I}_j)^n$ negligibly small. The approximation depends on the local nodal properties, which is typically valid locally for large degree nodes and high infected density of neighboring nodes. For the small-degree

nodes, the high-order terms in Eq. (32) can no longer be neglected. In general, the validity of the approximation for the whole network depends not only on the infection density but also on the network structure, and the approximate equivalence holds if the small-degree nodes are not abundant in the network. If there is an appreciable fraction of small-degree nodes in a strongly hetero-geneous network, the approximate equivalence would fail. Other-wise, the effective infection rate can be approximated as

$$\lambda_{\mathrm{eff}} \approx \lambda_{\mathrm{eff}}^{*}. \tag{40}$$

Furthermore, when the infection process is Markovian regardless of whether the recovery process remains non-Markovian or Marko-vian, there exists an equivalence between non-Markovian and Markovian types of SIS dynamics with the following equality (see Supplementary Note 1):

$$\lambda_{\mathrm{eff}} = \lambda_{\mathrm{eff}}^{*}. \tag{41}$$

For non-Markovian SIS dynamics which can be equivalent to Markovian dynamics, the outbreak threshold is given by[65]

$$\lambda_{c}^{\mathrm{eff}} = \frac{1}{\Lambda_{\max}}, \tag{42}$$

where $\Lambda_{\max}$ is the maximum eigenvalue of the network adjacency matrix. For processes with type-I mechanism where there is no equivalence between non-Markovian and Markovian dynamics, it is generally difficult to identify a relevant parameter to characterize the phase transition associated with disease outbreak.

To test when an equivalence between non-Markovian and Markovian spreading processes arises, we focus on the effects of the infection time distribution on the stationary infected density with both types of edge activation mechanisms. We first consider the case of type-II mechanism. We set $\alpha_{\mathrm{I}} = 0.5, 1, 2, 4$, $\alpha_{\mathrm{R}} = 2$, and $\beta_{\mathrm{R}} = 0.5$ and adjust λ_{eff} by changing β_{I} through Eq. (37). Figure 4 shows the simulation results on random, scale-free and Hamsterster networks, which are the same as the networks in Fig. 3. It can be seen that, regardless of the network structure, the stationary infected density agrees well with both the result from Markovian process simulation and the analytical solution of the Markovian dynamics from Eq. (39) or (36). The theoretical thresholds calculated from Eq. (42) on random, scale-free, and Hamsterster networks are 0.096, 0.040 and 0.020, respectively, which are quite close to the simulated values of the threshold in Fig. 4. (Supplementary Fig. 5 in Supplementary Note 6 provides a comparison of stationary probability density distribution between simulation and theoretical prediction).

We now turn to the type-I case. For $\alpha_{\mathrm{I}} = 1$, the distribution of infection time is exponential, making the underlying non-Markovian process completely equivalent to a Markovian process with the effective recovery rate δ_{eff} and effective infection rate λ_{eff} given by Eqs. (33) and (41), respectively. Indeed, we find that, as λ_{eff} is increased, or, equivalently, as β_{I} is decreased, the infected density for the non-Markovian process with type-I activation mechanism agrees with the theoretical value of the corresponding Markovian process (Supplementary Fig. 6 in Supplementary Note 7 shows the results). For $\alpha_{\mathrm{I}} \neq 1$, the exact equivalence breaks down. However, under certain conditions, an approximate equiva-lence can still be expected. To obtain the approximate equivalence, we analyze the effect of higher-order terms in Eq. (31) for non-Markovian process with type-I activation mechanism. For simplicity, we assume that $\psi_{\mathrm{rec}}(\tau)$ is from
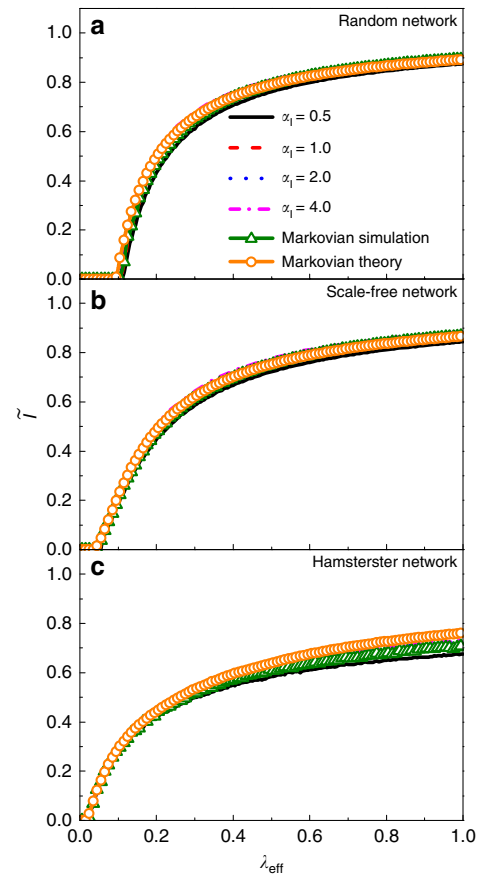
Fig. 4 Demonstration of equivalence. Comparison of stationary infected density with type-II activation mechanism between non-Markovian and Markovian processes for **a** random **b** scale-free, and **c** Hamsterster networks which are the same as the networks in Fig. 3. Solid, dashed, dotted, and dot-dashed curves represent the results for $\alpha_{\mathrm{I}} = 0.5, 1, 2, 4$, respectively, and the triangles and circles correspond to simulation results from the Markovian process and the analytical solutions, respectively. Other parameters are $\alpha_{\mathrm{R}} = 2$ and $\beta_{\mathrm{R}} = 0.5$

Eq. (22) but $\psi_{\mathrm{inf}}(\tau)$ is a Beta distribution:

$$\frac{1}{B(\sigma, \gamma)} \kappa^{\sigma-1}(1-\kappa)^{\gamma-1} \tag{43}$$

with $\sigma = 1$. We have

$$\psi_{\mathrm{inf}}(\kappa) = \gamma(1-\kappa)^{\gamma-1}, \tag{44}$$

where $0 \leq \kappa < 1$ and $\omega_{\mathrm{inf}}(\kappa) = \gamma/(1-\kappa)$. Especially, Eq. (44) turns into a uniform distribution $\psi_{\mathrm{inf}}(\kappa) = 1 (0 \leq \kappa < 1)$ for $\gamma = 1$. We set $\alpha_{\mathrm{R}} = 0.5, 1, 2, 4$ and $\beta_{\mathrm{R}} = 0.5$, and adjust $\vartheta^{(n)}(0)$ by changing the value of γ. From Eqs. (34), (31) and (44), for a fixed value of α_{R}, the proportional relationship among all $\vartheta^{(n)}(0)$ can remain invariant through a proper modification in the value of γ. In particular, an increase in the value of θ multiplying γ will result in an increase in the value of $\omega_{\mathrm{inf}}(\tau)$ by θ times. As a result, every value of $\Omega(\tau)$ will increase by the same factor θ. For $\forall n \geq 0$, the quantity $\vartheta^{(n)}(0)$ will decrease by the factor of θ, making the proportional relationship unchanged. From Eq. (40), we obtain the approximate effective infection rate as $\lambda_{\mathrm{eff}} \approx \gamma/\delta_{\mathrm{eff}}$. Figure 5 demonstrates a significant deviation in the stationary infected density, when its values are relatively small, of the
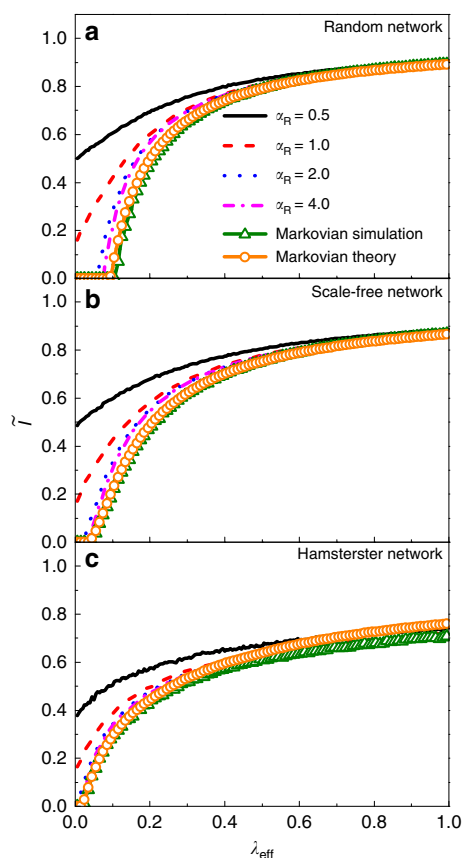
Fig. 5 Demonstration of approximate equivalence. Shown are the stationary infected density with type-I activation mechanism for **a** random, **b** scale-free, and **c** Hamsterster networks, which are the same as the networks in Fig. 3, for $\beta_R = 0.5$. Solid, dashed, dotted, and dot-dashed curves represent the results for $\alpha_R = 0.5, 1, 2, 4$, respectively. Triangles and circles denote the results from the Markovian process and its analytical solution, respectively. An approximate equivalence arises in the regime of large infected density

non-Markovian process from that of the Markovian process with the effective infection rate λ_{eff}. However, as the values of λ_{eff} and $\tilde{I}$ are increased, the results for the non-Markovian process gradually converge to those for the Markovian process. For a large value of α_R, the values of $\vartheta^{(n)}(0)$ for $n \geq 2$ are reduced, decreasing the gap between the results from the non-Markovian and Markovian processes. Simulation results on strong heterogeneous networks also verify these results (see Supplementary Fig. 7 in Supplementary Note 8 for details).

Discussion

Disease or virus spreading dynamics in networked systems in the real world are non-Markovian in that the temporal sequences of the occurrences of the key events underlying the spreading process do not follow a Poisson distribution. The non-Poisson behaviors make mathematical analyses of the spreading dynamics difficult, hindering their understanding. It is desired to develop a theoretical framework for non-Markovian spreading dynamics on complex networks. An issue of interest concerns about the inter-relation between non-Markovian and Markovian dynamics. Especially, while Markovian spreading processes with the Poisson characteristic are not a true reflection of real world situations, rigorous analyses and a relatively comprehensive understanding

of the underlying dynamics are possible, as demonstrated in the past two decades[5,7]. A curiosity driven and practically significant question is then under what conditions will a non-Markovian process be equivalent to a Markovian one. And, if such an equivalence does not exist, to what extent can a non-Markovian process be approximated by a Markovian one? In spite of previous work on non-Markovian spreading dynamics on complex networks[34,35,37,39–48], these issues have not been addressed satisfactorily, which motivated our current work.

We have developed a first-order mean field theory to solve both the transient phase and steady states of non-Markovian, SIS type of spreading dynamics. The theory can be used to assess accurately the difference between non-Markovian and Markovian dynamics, for any network structure. A finding is that, whether there is an equivalence between non-Markovian and Markovian processes depends on the specific edge activation mechanism. There are situations where non-Markovian SIS type of dynamics cannot be understood in terms of equivalent Markovian dynamics. We have identified one generic condition under which a complete equivalence between non-Markovian and Markovian processes holds: absence of any temporal correlation on active edges. When the correlation cannot be ignored due to the influence of susceptible nodes on active edges, the equivalence no longer holds. However, an approximate equivalence may still hold for the whole network, depending on the infection density and the network structure. We have found that, in the regime of relatively large infected density, a non-Markovian process can be approximated by a Markovian one for heterogeneous networks if small-degree nodes are not abundant in the network. All these findings were enabled by the theory developed in this paper.

While we have focused on non-Markovian, SIS type of spreading dynamics, a hope is that our mean-field theory can be extended to other types of dynamics such as SIR spreading or even cascading processes. Our work suggests the importance of accurately identifying the edge activation mechanisms responsible for spreading processes in the real world, which are key to determining whether an equivalence to Markovian dynamics exists so as to gain a deeper understanding of the underlying spreading process. Besides the two edge activation mechanisms, other types of edge activation mechanisms have been studied in the literature. For example, rule 2 in ref.[43] prescribes that the age of an active link is solely determined by the age of the infected node, which bears certain similarity but not identical to type-II edge activation studied in this paper. For this edge activation mechanism, an equivalence between non-Markovian and Markovian processes holds (see Supplementary Note 9 and Supplementary Figs. 8–10 for details). The issues of dynamical correlation and network communicability[66] are also critically important to non-Markovian spreading dynamics, for which a theoretical framework, e.g., a higher-order mean field framework, is lacking. An interesting question is whether the equivalence holds in the higher-order mean field framework or in a transient process. For example, when the system is in transient, the distribution of the state age varies with time, making invalid dimension reduction in the analysis of the infection and susceptible probabilities. At the present, it is not feasible to determine whether there is an equivalences between non-Markovian and Markovian processes in the transient regime.

Methods

Random number generation. Taking $\psi_{\mathrm{inf}}(\kappa)$ for example, its survival probability distribution is expressed as $\Psi_{\mathrm{inf}}(\kappa) = \int_{\kappa}^{+\infty} \psi_{\mathrm{inf}}(\kappa')\mathrm{d}\kappa'$. In order to obtain a random number κ, we generate a random number p uniformly distributed between zero and one and solve the equation

$$\Psi_{\mathrm{inf}}(\kappa) = p. \tag{45}$$

For the Weibull distribution in Eq. (21) and the Beta distribution in Eq. (44), the value of κ is given by

$$\kappa = \beta_{\mathrm{I}}(\ln\frac{1}{p})^{1/\alpha_{\mathrm{I}}} \tag{46}$$

and

$$\kappa = 1 - p^{1/\gamma}, \tag{47}$$

respectively. We calculate the elapsed time τ with the distribution $\psi_{\mathrm{rec}}(\tau)$ in a similar way.

Simulation method. In a network, each infected node or active edge is marked with an event-time defined as the absolute time when the infected node will recover or when the active edge will transmit the disease. The event-times of susceptible nodes and non-active edges are set as $+\infty$. All nodes and edges are assigned to a min-heap according to their event-times. Once the event-time of a node or an edge has changed, its position will be shifted in the min-heap instantaneously. Thus, the event-time of the node or edge at the root must be minimum. At each step, it is only necessary to make the node or edge at the root of the min-heap recover or transmit the disease[62], respectively.

For an infected node located at the root, meaning that the recovery event of the node will occur first among all the events including recovery and disease-transmitting events in the network, we update the absolute time t to the event-time of the node and let the node recover. The event-time of the node then turns into $+\infty$. This recovery event will lead to state changes of some edges connected to the node. If some edges become active, we assign them new event-times $\kappa + t$, where κ is a random number generated from the distribution $\psi_{\mathrm{inf}}(\kappa)$ and t is the current absolute time. The new event-time means the active edge will transmit disease at the absolute time $\kappa + t$. If some edges become non-active, their event-times become $+\infty$.

If an active edge is located at the root, i.e., the disease transmission event of the edge will occur first among all the events, we update the absolute time t to the event-time of the edge, and then let the edge transmit disease. This transmission event can lead to a series of state changes of some nodes or edges and, consequently, the event-times of the new active and non-active edges are renewed to $\kappa + t$ and $+\infty$, respectively. In addition, the event-time of a new infected node will be updated to $\tau + t$, where τ follows the distribution $\psi_{\mathrm{rec}}(\tau)$.

Data availability
The source data underlying Figs. 3–5 and Supplementary Figs. 2–9 are provided as a Source Data file.

Code availability
C++ code to reproduce the data in the main text and the Supplementary Information is available at https://github.com/fengmi9312/Codes-for-NCOMMS-19-00777.

References
1. Pastor-Satorras, R. & Vespignani, A. Epidemic spreading in scale-free networks. *Phys. Rev. Lett.* **86**, 3200 (2001).
2. Pastor-Satorras, R. & Vespignani, A. Epidemic dynamics and endemic states in complex networks. *Phys. Rev. E* **63**, 066117 (2001).
3. Vespignani, A. Predicting the behavior of techno-social systems. *Science* **325**, 425–428 (2009).
4. Vespignani, A. Modelling dynamical processes in complex socio-technical systems. *Nat. Phys.* **8**, 32–39 (2012).
5. Pastor-Satorras, R., Castellano, C., Van Mieghem, P. & Vespignani, A. Epidemic processes in complex networks. *Rev. Mod. Phys.* **87**, 925 (2015).
6. Domenico, M. D., Granell, C., Porter, M. & Arenas, A. The physics of spreading processes in multilayer networks. *Nat. Phys.* **12**, 901–906 (2016).
7. Wang, W., Tang, M., Stanley, H. E. & Braunstein, L. A. Unification of theoretical approaches for epidemic spreading on complex networks. *Rep. Prog. Phys.* **80**, 036603 (2017).
8. Nematzadeh, A., Ferrara, E., Flammini, A. & Ahn, Y.-Y. Optimal network modularity for information diffusion. *Phys. Rev. Lett.* **113**, 088701 (2014).
9. Anderson, R. M. & May, R. M. *Infectious Diseases of Humans: Dynamics and Control* (Oxford University Press, Oxford, 1992).
10. Van Mieghem, P., Omic, J. & Kooij, R. Virus spread in networks. *IEEE/ACM Trans. Net. (TON)* **17**, 1–14 (2009).
11. Van Mieghem, P. The n-intertwined SIS epidemic network model. *Computing* **93**, 147–169 (2011).
12. Barabasi, A.-L. The origin of bursts and heavy tails in human dynamics. *Nature* **435**, 207–211 (2005).
13. Stouffer, D. B., Malmgren, R. D. & Amaral, L. A. Comment on Barabasi. *Nature* **435**, 207 (2005). *arXiv preprint physics/0510216* (2005).
14. Vázquez, A. et al. Modeling bursts and heavy tails in human dynamics. *Phys. Rev. E* **73**, 036127 (2006).
15. Brockmann, D., Hufnagel, L. & Geisel, T. The scaling laws of human travel. *Nature* **439**, 462–465 (2006).
16. González, M. C., Hidalgo, C. A. & Barabási, A. L. Understanding individual human mobility patterns. *Nature* **453**, 779–782 (2008).
17. Song, C., Koren, T., Wang, P. & Barabási, A. L. Modelling the scaling properties of human mobility. *Nat. Phys.* **6**, 818–823 (2010).
18. Eagle, N., Macy, M. & Claxton, R. Network diversity and economic development. *Science* **328**, 1029–1031 (2010).
19. Hu, Y., Zhang, J., Huan, D. & Di, Z.-R. Toward a general understanding of the scaling laws in human and animal mobility. *Europhys. Lett.* **96**, 38006 (2011).
20. Noulas, A., Scellato, S., Lambiotte, R., Pontil, M. & Mascolo, C. A tale of many cities: universal patterns in human urban mobility. *PLoS ONE* **7**, e37027 (2012).
21. Lenormand, M., Huet, S., Gargiulo, F. & Deffuant, G. A universal model of commuting networks. *PLoS ONE* **7**, e45985 (2012).
22. Goh, S., Lee, K., Park, J. S. & Choi, M. Y. Modification of the gravity model and application to the metropolitan Seoul subway system. *Phys. Rev. E* **86**, 026102 (2012).
23. Simini, F., González, M. C., Maritan, A. & Barabási, A. L. A universal model for mobility and migration patterns. *Nature* **484**, 96–100 (2012).
24. Saramäki, J. et al. Persistence of social signatures in human communication. *Proc. Natl Acad. Sci.* **111**, 942–947 (2013).
25. Simini, F., Maritan, A. & Néda, Z. Human mobility in a continuum approach. *PLoS ONE* **8**, e60069 (2013).
26. Ren, Y., Ercsey-Ravasz, M., Wang, P., González, M. C. & Toroczkai, Z. Predicting commuter flows in spatial networks using a radiation model based on temporal ranges. *Nat. Commun.* **5**, 5347 (2014).
27. Zhao, Z.-D., Huang, Z.-G., Huang, L., Liu, H. & Lai, Y.-C. Scaling and correlation of human movements in cyber and physical spaces. *Phys. Rev. E* **90**, 050802(R) (2014).
28. Yan, X.-Y., Zhao, C., Fan, Y., Di, Z.-R. & Wang, W.-X. Universal predictability of mobility patterns in cities. *J. R. Soc. Interface* **11**, 20140834 (2014).
29. Šćepanović, S., Mishkovski, I., Hui, P., Nurminen, J. K. & Ylä-Jääski, A. Mobile phone call data as a regional socio-economic proxy indicator. *PLoS ONE* **10**, e0124160 (2015).
30. Pappalardo, L. et al. Returners and explorers dichotomy in human mobility. *Nat. Commun.* **6**, 8166 (2015).
31. Gallotti, R., Bazzani, A., Rambaldi, S. & Barthelemy, M. A stochastic model of randomly accelerated walkers for human mobility. *Nat. Commun.* **7**, 12600 (2016).
32. Zhao, Y.-M., Zeng, A., Yan, X.-Y., Wang, W.-X. & Lai, Y.-C. Unified underpinning of human mobility in the real world and cyberspace. *New J. Phys.* **18**, 053025 (2016).
33. Yan, X.-Y., Wang, W.-X., Gao, Z.-Y. & Lai, Y.-C. Universal model of individual and population mobility on diverse spatial scales. *Nat. Commun.* **8**, 1639 (2017).
34. Kenah, E. & Robins, J. M. Second look at the spread of epidemics on networks. *Phys. Rev. E* **76**, 036113 (2007).
35. Vazquez, A., Racz, B., Lukacs, A. & Barabasi, A.-L. Impact of non-poissonian activity patterns on spreading processes. *Phys. Rev. Lett.* **98**, 158702 (2007).
36. Iribarren, J. & Moro, E. Impact of human activity patterns on the dynamics of information diffusion. *Phys. Rev. Lett.* **103**, 038702 (2009).
37. Karrer, B. & Newman, M. E. J. Message passing approach for general epidemic models. *Phys. Rev. E* **82**, 016101 (2010).
38. Iribarren, J. & Moro, E. Branching dynamics of viral information spreading. *Phys. Rev. E* **84**, 046116 (2011).
39. Min, B., Goh, K.-I. & Vazquez, A. Spreading dynamics following bursty human activity patterns. *Phys. Rev. E* **83**, 036102 (2011).
40. Min, B., Goh, K.-I. & Kim, I.-M. Suppression of epidemic outbreaks with heavy-tailed contact dynamics. *Europhys. Lett.* **103**, 50002 (2013).
41. Van Mieghem, P. & van de Bovenkamp, R. Non-markovian infection spread dramatically alters the susceptible-infected-susceptible epidemic threshold in networks. *Phys. Rev. Lett.* **110**, 108701 (2013).
42. Cator, E., van de Bovenkamp, R. & Van Mieghem, P. Susceptible-infected-susceptible epidemics on networks with general infection and cure times. *Phys. Rev. E* **87**, 062816 (2013).
43. Boguná, M., Lafuerza, L. F., Toral, R. & Serrano, M. Á. Simulating non-markovian stochastic processes. *Phys. Rev. E* **90**, 042108 (2014).
44. Jo, H.-H., Perotti, J. I., Kaski, K. & Kertész, J. Analytically solvable model of spreading dynamics with non-poissonian processes. *Phys. Rev. X* **4**, 011041 (2014).

45. Georgiou, N., Kiss, I. Z. & Scalas, E. Solvable non-markovian dynamic network. *Phys. Rev. E* **92**, 042801 (2015).

46. Kiss, I. Z., Röst, G. & Vizi, Z. Generalization of pairwise models to non-markovian epidemics on networks. *Phys. Rev. Lett.* **115**, 078701 (2015).

47. Starnini, M., Gleeson, J. P. & Boguñá, M. Equivalence between non-markovian and markovian dynamics in epidemic spreading processes. *Phys. Rev. Lett.* **118**, 128301 (2017).

48. Sherborne, N., Miller, J., Blyuss, K. & Kiss, I. Mean-field models for non-markovian epidemics on networks. *J. Math. Biol.* **76**, 755–558 (2018).

49. Valdano, E., Ferreri, L., Poletto, C. & Colizza, V. Analytical computation of the epidemic threshold on temporal networks. *Phys. Rev. X* **5**, 021005 (2015).

50. Valdano, E., Fiorentin, M. R., Poletto, C. & Colizza, V. Epidemic threshold in continuous-time evolving networks. *Phys. Rev. Lett.* **120**, 068302 (2018).

51. Rand, D. A. in *Advanced Ecological Theory: Principles and Applications* (ed. McGlade, J.) 100–142 (Wiley, Hoboken, NJ, USA, 1999).

52. Keeling, M. J. The effects of local spatial structure on epidemiological invasions. *Proc. R. Soc. Lond. B Biol. Sci.* **266**, 859–867 (1999).

53. Keeling, M. J. & Rand, D. A. in *From Finite to Infinite Dimensional Dynamical Systems* (eds Robinson, J. C. & Glendinning, P. A.) 5–57 (Springer, Germany, 2001).

54. Eames, K. T. & Keeling, M. J. Modeling dynamic and network heterogeneities in the spread of sexually transmitted diseases. *Proc. Natl Acad. Sci. USA* **99**, 13330–13335 (2002).

55. Gleeson, J. P. High-accuracy approximation of binary-state dynamics on networks. *Phys. Rev. Lett.* **107**, 068701 (2011).

56. Lai, Y.-C. & Tél, T. *Transient Chaos - Complex Dynamics on Finite-Time Scales*. 1st edn (Springer, New York, 2011).

57. Hastings, A. & Higgins, K. Persistence of transients in spatially structured ecological models. *Science* **263**, 1133–1136 (1994).

58. Hastings, A. Transient dynamics and persistence of ecological systems. *Ecol. Lett.* **4**, 215–220 (2001).

59. Hastings, A. Transients: the key to long-term ecological understanding? *Trends Ecol. Evol.* **19**, 39–45 (2004).

60. Hastings, A. Timescales and the management of ecological systems. *Proc. Natl Acad. Sci. USA* **113**, 14568–14573 (2016).

61. Hastings, A. et al. Transient phenomena in ecology. *Science* **361**, eaat6412 (2018).

62. Gibson, M. A. & Bruck, J. Efficient exact stochastic simulation of chemical systems with many species and many channels. *J. Phys. Chem. A.* **104**, 1876–1889 (2000).

63. Hamsterster full network dataset – KONECT (2017). http://konect.uni-koblenz.de/networks/petster-hamster.

64. Van Mieghem, P. *Performance Analysis of Communications Networks and Systems* (Cambridge University Press, Cambridge, UK, 2009).

65. Chakrabarti, D., Wang, Y., Wang, C., Leskovec, J. & Faloutsos, C. Epidemic thresholds in real networks. *ACM Trans. Info Sys. Secu.* **10**, 1 (2008).

66. Estrada, E., Hatanoe, N. & Benzi, M. The physics of communicability in complex networks. *Phys. Rep.* **514**, 89–119 (2012).

Author contributions

M.F. and M.T. designed research; M.F. performed research; S.-M.C., M.T., and Y.-C.L. contributed analytic tools; M.F., S.-M.C., M.T., and Y.-C.L. analyzed data; M.F., M.T., and Y.-C.L. wrote the paper.

Additional information

Competing interests: The authors declare no competing interests.

Peer review information: *Nature Communications* thanks the anonymous reviewers for their contribution to the peer review of this work. Peer reviewer reports are available.

Publisher's note: Springer Nature remains neutral with regard to jurisdictional claims in published maps and institutional affiliations.

Supplementary Information for

Equivalence and its invalidation between Non-Markovian and Markovian spreading dynamics on complex networks

Mi Feng, Shimin Cai, Ming Tang, and Ying-Cheng Lai

Corresponding author: Ming Tang (tangminghan007@gmail.com)

SUPPLEMENTARY NOTE 1. STEADY STATE SOLUTION OF NON-MARKOVIAN SIS MODEL WITH TYPE-I ACTIVATION MECHANISM

When the system reaches a steady state, the differential equations governing the evolution of the probability density functions of node i in the infected and susceptible states are, respectively,

$$\frac{d\tilde{I}_i(\tau)}{d\tau} = -\omega_{\text{rec}}(\tau)\tilde{I}_i(\tau) \ \text{ and} \tag{1}$$

$$\frac{d\tilde{S}_i(\tau)}{d\tau} = -\tilde{S}_i(\tau)\sum_{j=1}^{N} a_{ij} \int_0^{+\infty} \omega_{\text{inf}}[\min(\tau,\tau')]\tilde{I}_j(\tau')d\tau', \tag{2}$$

with the initial condition

$$\tilde{I}_i(0) = \tilde{S}_i(0). \tag{3}$$

From Supplementary Eq. (1), we have

$$\tilde{I}_i(\tau) = \tilde{I}_i(0)\Psi_{\text{rec}}(\tau), \tag{4}$$

where $\Psi_{\text{rec}}(\tau) = e^{-\int_0^\tau \omega_{\text{rec}}(\tau')d\tau'}$. From Supplementary Eq. (2), we have

$$\tilde{S}_i(\tau) = \tilde{S}_i(0)e^{-\int_0^\tau \sum_{j=1}^N a_{ij} \int_0^{+\infty} \omega_{\text{inf}}[\min(\tau',\tau'')]\tilde{I}_j(\tau')d\tau'd\tau''}. \tag{5}$$

Substituting, respectively, Supplementary Eqs. (4) and (5) into

$$\tilde{I}_i = \int_0^{+\infty} \tilde{I}_i(\tau)d\tau \ \text{ and} \ \ \tilde{S}_i = \int_0^{+\infty} \tilde{S}_i(\tau)d\tau, \tag{6}$$

we obtain the stationary distribution of node i being in the infected and susceptible state, respectively, as

$$\tilde{I}_i = \tilde{I}_i(0) \int_0^{+\infty} \Psi_{\text{rec}}(\tau)d\tau \ \text{ and} \tag{7}$$

$$\tilde{S}_i = \tilde{S}_i(0) \int_0^{+\infty} e^{-\int_0^\tau \sum_{j=1}^N a_{ij} \int_0^{+\infty} \omega_{\text{inf}}[\min(\tau',\tau'')]\tilde{I}_i(\tau')d\tau'd\tau''}d\tau. \tag{8}$$

Defining the effective recovery rate as

$$\delta_{\text{eff}} = 1/\int_0^{+\infty} \Psi_{\text{rec}}(\tau)d\tau, \tag{9}$$

we can reduce Supplementary Eq. (7) to

$$\tilde{I}_i = \frac{\tilde{I}_i(0)}{\delta_{\text{eff}}}. \tag{10}$$

Combining Supplementary Eqs. (4) and (10), we obtain

$$\tilde{I}_i(\tau) = \tilde{I}_i\delta_{\text{eff}}\Psi_{\text{rec}}(\tau). \tag{11}$$

Equation (8) can then be rewritten as

$$\tilde{S}_i = \tilde{S}_i(0) \int_0^{+\infty} e^{-\delta_{\text{eff}} \int_0^\tau \int_0^{+\infty} \omega_{\text{inf}}[\min(\tau',\tau'')]\Psi_{\text{rec}}(\tau')d\tau'd\tau'' \sum_{j=1}^N a_{ij}\tilde{I}_j}\,d\tau. \tag{12}$$

Dividing Supplementary Eq. (10) by Supplementary Eq. (12) and using the initial condition Supplementary Eq. (3), we obtain

$$\delta_{\text{eff}}\tilde{I}_i = \frac{\tilde{S}_i}{\int_0^{+\infty} e^{-\delta_{\text{eff}} \int_0^\tau \int_0^{+\infty} \omega_{\text{inf}}[\min(\tau',\tau'')]\Psi_{\text{rec}}(\tau')d\tau'd\tau'' \sum_{j=1}^N a_{ij}\tilde{I}_j}\,d\tau}, \tag{13}$$

which can be further reduced to

$$\tilde{I}_i = \frac{\tilde{S}_i}{\delta_{\text{eff}} \int_0^{+\infty} e^{-\Omega(\tau)\sum_{j=1}^N a_{ij}\tilde{I}_j}\,d\tau}, \tag{14}$$

where

$$\Omega(\tau) = \delta_{\text{eff}} \int_0^\tau \int_0^{+\infty} \omega_{\text{inf}}[\min(\tau',\tau'')]\Psi_{\text{rec}}(\tau')d\tau'd\tau''. \tag{15}$$

Note that $\Omega(0) = 0$. Defining $\vartheta(\tau)$ as the inverse function of $\Omega(\tau)$, we have $\vartheta(0) = 0$. Equation (14) can be rewritten as

$$\tilde{I}_i = \frac{\tilde{S}_i}{\delta_{\text{eff}} \int_0^{+\infty} e^{-\xi}d[\vartheta(\frac{\xi}{\sum_{j=1}^N a_{ij}\tilde{I}_j})]}, \tag{16}$$

where $\xi = \Omega(\tau)\sum_{j=1}^N a_{ij}\tilde{I}_j$. Expanding $\vartheta(\tau)$ as a Taylor series about $\tau = 0$, we have

$$\vartheta(\frac{\xi}{\sum_{j=1}^N a_{ij}\tilde{I}_j}) = \vartheta(0) + \sum_{n=1}^{+\infty} \frac{1}{n!}\vartheta^{(n)}(0)(\frac{\xi}{\sum_{j=1}^N a_{ij}\tilde{I}_j})^n, \tag{17}$$

where $\vartheta(0) = 0$ and $\vartheta^{(n)}(0)$ is the nth derivative of $\vartheta^{(n)}(\tau)$. Note that, in order to have meaningful solutions, the right side of Supplementary Eq. (17) must converge. Combining Supplementary Eqs. (16) and (17), we obtain

$$\tilde{I}_i = \frac{\tilde{S}_i}{\delta_{\text{eff}} \int_0^{+\infty} e^{-\xi}d[\sum_{n=1}^{+\infty} \frac{1}{n!}\vartheta^{(n)}(0)(\frac{\xi}{\sum_{j=1}^N a_{ij}\tilde{I}_j})^n]}, \tag{18}$$

which can be rearranged as

$$\tilde{I}_i = \frac{\tilde{S}_i}{\delta_{\text{eff}} \sum_{n=1}^{+\infty} \frac{1}{(n-1)!}\vartheta^{(n)}(0)(\frac{1}{\sum_{j=1}^N a_{ij}\tilde{I}_j})^n \int_0^{+\infty} \xi^{n-1}e^{-\xi}d\xi}. \tag{19}$$

Using the property of the gamma function

$$\Gamma(n) \equiv \int_0^{+\infty} \xi^{n-1}e^{-\xi}d\xi = (n-1)!, \tag{20}$$

3

we have

$$\tilde{I}_i = \frac{\tilde{S}_i}{\delta_{\text{eff}} \sum_{n=1}^{+\infty} \vartheta^{(n)}(0)(\frac{1}{\sum_{j=1}^{N} a_{ij}\tilde{I}_j})^n}, \tag{21}$$

or

$$\frac{1}{\tilde{I}_i} = \frac{1}{\tilde{S}_i} \sum_{n=1}^{+\infty} \delta_{\text{eff}} \vartheta^{(n)}(0)(\frac{1}{\sum_{j=1}^{N} a_{ij}\tilde{I}_j})^n. \tag{22}$$

The higher order derivatives of the inverse function $\vartheta(\tau)$ can be calculated as [1]

$$\vartheta^{(1)}(0) = \frac{1}{\Omega^{(1)}(0)}. \tag{23}$$

For $n \geq 2$, we have

$$\vartheta^{(n)}(0) = \lim_{\Delta x \to 0} n! \frac{\Delta x - \sum_{i=1}^{n-1} \frac{1}{i!}(\vartheta^{(i)}(0))[\sum_{j=1}^{n} \frac{1}{j!}(\Omega^{(j)}(0))(\Delta x)^j]^i}{[\sum_{i=1}^{n} \frac{1}{i!}(\vartheta^{(i)}(0))(\Delta x)^i]^n}. \tag{24}$$

For the non-Markovian dynamics to be equivalent to Markovian, it is necessary that Supplementary Eq. (22) be reduced to the form of the steady state equation for Markovian spreading dynamics. The necessary condition is then that the quantity $\vartheta^{(n)}(0)$ must be zero for $\forall n > 1$. In this case, Supplementary Eq. (22) can be rewritten as

$$\frac{1}{\tilde{I}_i} = \frac{\delta_{\text{eff}} \vartheta^{(1)}(0)}{\tilde{S}_i \sum_{j=1}^{N} a_{ij}\tilde{I}_j}, \tag{25}$$

Since $\vartheta^{(1)}(0)$ is a finite value, we have $\vartheta(\tau) = \vartheta^{(1)}(0)\tau$. The inverse function of $\vartheta(\tau)$ is $\Omega(\tau) = \tau/\vartheta^{(1)}(0)$. From Supplementary Eq. (15), we get the first-order and second-order derivatives of $\Omega(\tau)$ as

$$\Omega'(\tau) = \delta_{\text{eff}} \int_0^\tau \omega_{\text{inf}}(\tau')\Psi_{\text{rec}}(\tau')d\tau' + \delta_{\text{eff}} \int_\tau^{+\infty} \omega_{\text{inf}}(\tau)\Psi_{\text{rec}}(\tau')d\tau' = \frac{1}{\vartheta^{(1)}(0)} \tag{26}$$

and

$$\Omega''(\tau) = \delta_{\text{eff}} \omega'_{\text{inf}}(\tau) \int_\tau^{+\infty} \Psi_{\text{rec}}(\tau')d\tau' = 0. \tag{27}$$

Because $\int_\tau^{+\infty} \Psi_{\text{rec}}(\tau')d\tau'$ is a monotonically decreasing function of τ in Supplementary Eq. (27), we have $\omega'_{\text{inf}}(\tau) = 0$ and $\omega_{\text{inf}}(\tau) = 1/\vartheta^{(1)}(0)$ while the integral $\int_\tau^{+\infty} \Psi_{\text{rec}}(\tau')d\tau'$ does not decrease to zero. Using the fact that the infection time distribution follows the distribution

$$\psi_{\text{inf}}(\kappa) = \omega_{\text{inf}}(\kappa)e^{-\int_0^\kappa \omega_{\text{inf}}(\kappa')d\kappa'}, \tag{28}$$

we have

$$\psi_{\text{inf}}(\tau) = \frac{1}{\vartheta^{(1)}(0)} e^{\frac{-\tau}{\vartheta^{(1)}(0)}}, \tag{29}$$

which is an exponential time distribution typical of a Markovian process and strictly follows the stationary state of Supplementary Eq. (25). If, for $\tau = \tau_0$, the following integral vanishes,

$$\int_{\tau_0}^{+\infty} \Psi_{\text{rec}}(\tau')d\tau' = 0, \tag{30}$$

4

we then have $\omega'_{\text{inf}}(\tau_0) \neq 0$ and $\omega_{\text{inf}}(\tau_0) \neq 1/\vartheta^{(1)}(0)$. However, in this case the quantities $\omega'_{\text{inf}}(\tau_0)$ and $\omega_{\text{inf}}(\tau_0)$ are not physically meaningful because an infected node has recovered when the value of the integral $\int_\tau^{+\infty} \Psi_{\text{rec}}(\tau')d\tau'$ decreases to zero. Taken together, the analysis enables us to draw the conclusion that, for SIS processes with type-I activation mechanism, only when the infection times are distributed exponentially will the whole process be equivalent to a Markovian process.

SUPPLEMENTARY NOTE 2. THEORETICAL ANALYSIS OF NON-MARKOVIAN SIS MODEL WITH TYPE-II ACTIVATION MECHANISM

We first derive the infection rate $\eta(\tau)$ of infected node j of age τ. Define $A_{l \leftarrow i}(\kappa, \tau; t)$ as the two-dimensional probability density function that the edge $l \leftarrow i$ is active with age κ and the infection age of node i is τ. The probability density function that node i stays in the infected state aged τ at time t is given by

$$I_i(\tau; t) = \lim_{\Delta\kappa \to 0} \sum_{n=0}^{\frac{\tau}{\Delta\kappa}} A_{l \leftarrow i}(n\Delta\kappa, \tau; t)\Delta\kappa = \int_0^\tau A_{l \leftarrow i}(\kappa, \tau; t)d\kappa, \tag{31}$$

It is worth noting that, for $\tau = 0$, the following equality holds:

$$I_i(0; t) = \lim_{\Delta\kappa \to 0} A_{l \leftarrow i}(0, 0; t)\Delta\kappa = A_{l \leftarrow i}(0, 0; t)d\kappa. \tag{32}$$

At time t, the probability that the edge $l \leftarrow i$ is active with age ranging from κ to $\kappa + d\kappa$ and node i is in the infected state with infection age in the interval $(\tau, \tau + d\tau)$ is $A_{l \leftarrow i}(\kappa, \tau, t)d\kappa d\tau$. In this case, node i returns to the susceptible state with probability $\omega_{\text{rec}}(\tau)d\tau$. The evolution equation of $I_i(\tau; t)$ is

$$(\frac{\partial}{\partial\tau} + \frac{\partial}{\partial t})I_i(\tau; t) = -\omega_{\text{rec}}(\tau)I_i(\tau; t). \tag{33}$$

The probability that the edge $l \leftarrow i$ transmits disease outward is $\omega_{\text{inf}}(\kappa)d\kappa$. The probability that neither recovery nor transmission occurs is $1 - \omega_{\text{rec}}(\tau)d\tau - \omega_{\text{inf}}(\kappa)d\kappa$. The evolution equation of $A_{l \leftarrow i}(\kappa, \tau; t)$ can then be written as

$$(\frac{\partial}{\partial\kappa} + \frac{\partial}{\partial\tau} + \frac{\partial}{\partial t})A_{l \leftarrow i}(\kappa, \tau; t) = -[\omega_{\text{inf}}(\kappa) + \omega_{\text{rec}}(\tau)]A_{l \leftarrow i}(\kappa, \tau; t). \tag{34}$$

Since an infected node i with infection age in the range from zero to $+\infty$ can transition into the susceptible state aged zero insofar as recovery is possible, we obtain the probability density function that node i returns to the susceptible state of zero age as

$$S_i(0; t + dt) = \int_0^{+\infty} \int_0^\tau \omega_{\text{rec}}(\tau)A_{l \leftarrow i}(\kappa, \tau; t)d\kappa d\tau. \tag{35}$$

To describe the time evolution of $S_i(\tau; t)$, we assume that the ages of two connected nodes are uncorrelated, and thus $\Phi_{i \leftarrow j}(\tau; t)$ is the probability density function that node i in the susceptible state of age τ is infected by node j at time t. During the period $(t, t + dt)$, a susceptible node i aged τ is infected by its neighbors with probability $\sum_{j=1}^N a_{ij}\Phi_{i \leftarrow j}(\tau; t)d\tau$,

5
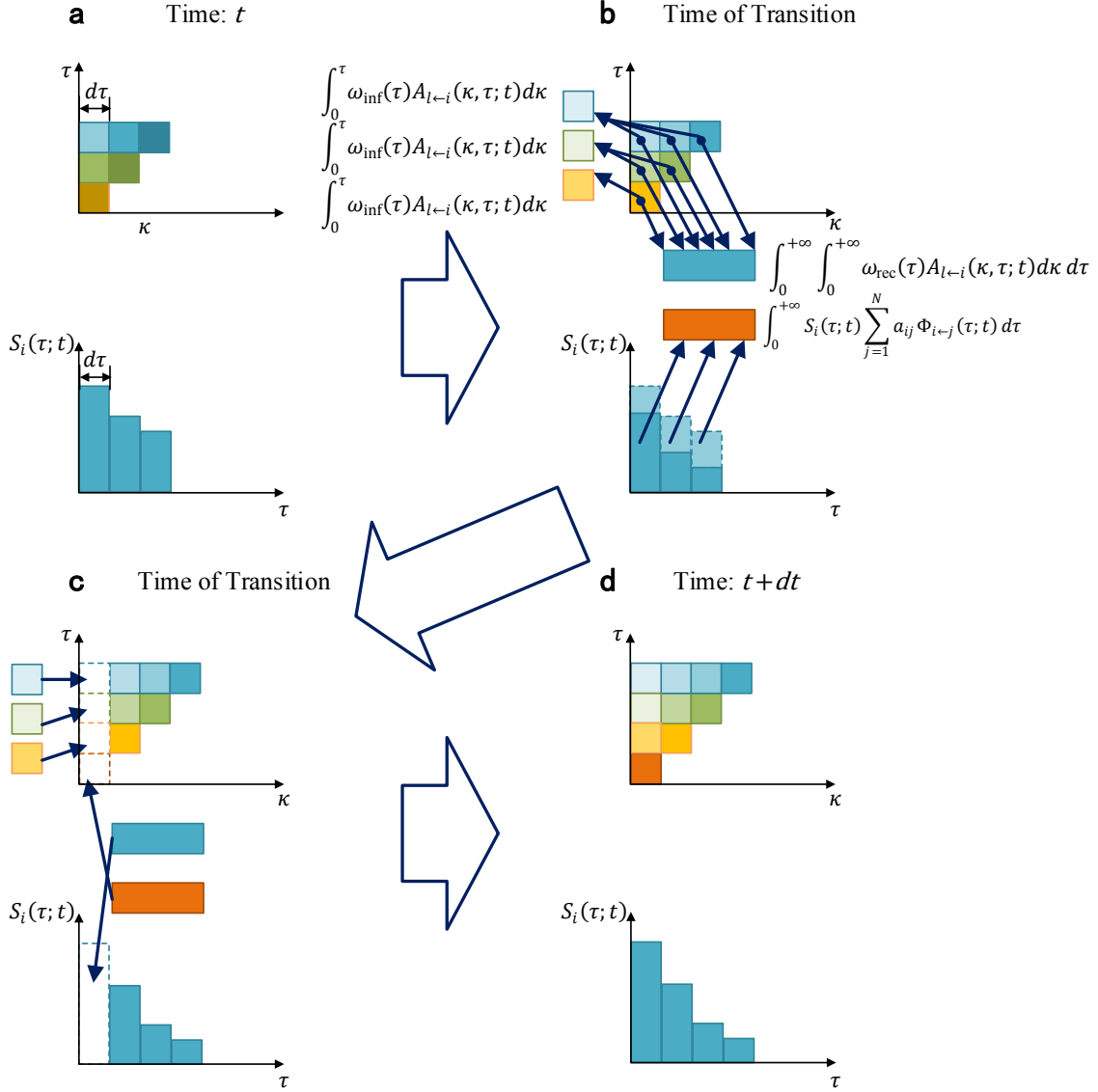
Supplementary Figure 1. Mechanism of probability flows with type-II activation mechanism. The magnitude of $A_{l\leftarrow i}(\kappa,\tau;t)$ is represented by the color of the squares, where a darker color indicates a larger value. **a** At time t, there are two distributions, $A_{l\leftarrow i}(\kappa,\tau;t)$ and $S_i(\tau;t)$. **b** Each square in $A_{l\leftarrow i}(\kappa,\tau;t)$ loses probability densities $\omega_{\mathrm{inf}}(\kappa)d\kappa A_{l\leftarrow i}(\kappa,\tau;t)$ and $\omega_{\mathrm{rec}}(\tau)d\tau A_{l\leftarrow i}(\kappa,\tau;t)$, and converges in the integrals $\int_0^\tau \omega_{\mathrm{inf}}(\tau)A_{l\leftarrow i}(\kappa,\tau;t)d\kappa$ and $\int_0^{+\infty}\int_0^\tau \omega_{\mathrm{rec}}(\tau)A_{l\leftarrow i}(\kappa,\tau;t)d\kappa d\tau$. Each block of $S_i(\tau;t)$ losses probability density $S_i(\tau,t)\sum_{j=1}^N a_{ij}\Phi_{i\leftarrow j}(\tau;t)d\tau$ and converges in the integral $\int_0^{+\infty} S_i(\tau,t)\sum_{j=1}^N a_{ij}\Phi_{i\leftarrow j}(\tau;t)d\tau$. **c** An amount of the density $\int_0^{+\infty}\int_0^\tau \omega_{\mathrm{rec}}(\tau)A_{l\leftarrow i}(\kappa,\tau;t)d\kappa d\tau$ flows into the susceptible state, i.e., $S_i(0;t+dt)$, an amount $\int_0^\tau \omega_{\mathrm{inf}}(\tau)A_{l\leftarrow i}(\kappa,\tau;t)d\kappa$ flows into the ordinate axis of $A_{l\leftarrow i}(\kappa,\tau;t+dt)$, i.e., $A_{l\leftarrow i}(0,\tau+d\tau;t+dt)$, $\int_0^{+\infty} S_i(\tau,t)\sum_{j=1}^N a_{ij}\Phi_{i\leftarrow j}(\tau;t)d\tau$ flows into the infected state: $A_{l\leftarrow i}(0,0;t+dt)$. **d** A series of probabilities flows results in two distributions $A_{l\leftarrow i}(\kappa,\tau;t=dt)$ and $S_i(\tau;t+dt)$ at time $t+dt$.

where N is the network size and a_{ij} is the element of the network adjacency matrix. We thus have

$$\left(\frac{\partial}{\partial \tau} + \frac{\partial}{\partial t}\right)S_i(\tau;t) = -S_i(\tau;t)\sum_{j=1}^{N} a_{ij}\Phi_{i\leftarrow j}(\tau;t), \tag{36}$$

where

$$\Phi_{i\leftarrow j}(\tau;t) = \int_0^\tau \int_0^{\tau'} \omega_{\text{inf}}(\kappa)A_{i\leftarrow j}(\kappa,\tau';t)d\kappa d\tau'. \tag{37}$$

Regardless of the value of the active age, from zero to ∞, of the edge $l \leftarrow i$ in the active state, if it propagates the disease, it is still in the active state but of age zero. We thus have

$$A_{l\leftarrow i}(0,\tau+d\tau;t+dt) = \int_0^\tau \omega_{\text{inf}}(\tau)A_{l\leftarrow i}(\kappa,\tau;t)d\kappa. \tag{38}$$

Since a susceptible node i with any susceptibility age ranging from zero to ∞ can transition into the infected state aged zero insofar as the infection process occurs, we obtain the probability density function that the edge $l \leftarrow i$ becomes the active state aged $\tau = \kappa = 0$ as

$$A_{l\leftarrow i}(0,0;t+dt) = \int_0^{+\infty} S_i(\tau;t)\sum_{j=1}^{N} a_{ij}\Phi_{i\leftarrow j}(\tau;t)d\tau. \tag{39}$$

Supplementary Fig. 1 illustrates the probability flow between $A_{l\leftarrow i}(\kappa,\tau;t)$ and $S_i(\tau;t)$ and those in their respective interiors. To reduce the dimension of the evolution equations, we define

$$\eta(\tau;t) = \frac{\int_0^\tau \omega_{\text{inf}}(\kappa)A_{i\leftarrow j}(\kappa,\tau;t)d\kappa}{I_j(\tau;t)}, \tag{40}$$

which is the infection rate $\eta(\tau;t)$ of an infected node j aged τ at time t. Equation (37) can be rewritten as

$$\Phi_{i\leftarrow j}(\tau;t) = \int_0^\tau \eta(\tau';t)I_j(\tau';t)d\tau'. \tag{41}$$

From Supplementary Eq. (34), we get

$$A_{i\leftarrow j}(\kappa,\tau;t) = A_{i\leftarrow j}(0,\tau-\kappa;t-\kappa)e^{-\int_0^\kappa \omega_{\text{inf}}\tau' + \omega_{\text{rec}}(\tau-\kappa-\tau')d\tau'}. \tag{42}$$

Because of the relations $\Psi_{\text{rec}}(\tau) = e^{-\int_0^\tau \omega_{\text{rec}}(\tau')d\tau'}$ and $\Psi_{\text{inf}}(\kappa) = e^{-\int_0^\kappa \omega_{\text{inf}}(\kappa')d\kappa'}$, we can rewrite Supplementary Eq. (42) as

$$A_{i\leftarrow j}(\kappa,\tau;t) = A_{i\leftarrow j}(0,\tau-\kappa;t-\kappa)\Psi_{\text{inf}}(\kappa)\frac{\Psi_{\text{rec}}(\tau)}{\Psi_{\text{rec}}(\tau-\kappa)}. \tag{43}$$

Equation (38) can then be rewritten as

$$A_{i\leftarrow j}(0,\tau+d\tau;t+dt) = \int_0^\tau \omega_{\text{inf}}(\kappa)A_{i\leftarrow j}(0,\tau-\kappa;t-\kappa)\Psi_{\text{inf}}(\kappa)\frac{\Psi_{\text{rec}}(\tau)}{\Psi_{\text{rec}}(\tau-\kappa)}d\kappa. \tag{44}$$

Dividing both sides of the equation by $I_j(\tau;t) = I_j(0;t-\tau)\Psi_{\text{rec}}(\tau)$ [from Supplementary Eq. (33)] and combining it with Supplementary Eq. (38), we have

$$\eta(\tau;t) = \frac{A_{i\leftarrow j}(0,\tau+d\tau;t+dt)}{I_j(0;t-\tau)\Psi_{\text{rec}}(\tau)} = \int_0^\tau \frac{A_{i\leftarrow j}(0,\tau-\kappa;t-\kappa)\psi_{\text{inf}}(\kappa)}{I_j(0;t-\tau)\Psi_{\text{rec}}(\tau-\kappa)}d\kappa. \tag{45}$$

From Supplementary Eqs. (32) and (38) as well as the condition $\Psi_{\text{rec}}(0) = 1$, we get

$$
\begin{aligned}
\eta(\tau;t) &= \int_0^{\tau-d\tau} \frac{A_{i\leftarrow j}(0,\tau-\kappa;t-\kappa)\psi_{\text{inf}}(\kappa)}{I_j(0;t-\tau)\Psi_{\text{rec}}(\tau-\kappa)} d\kappa + \psi_{\text{inf}}(\tau) \\
&= \int_{d\tau}^{\tau} \frac{A_{i\leftarrow j}(0,\tau+d\tau-\kappa;t+dt-\kappa)\psi_{\text{inf}}(\kappa-d\tau)}{I_j(0;t-\tau)\Psi_{\text{rec}}(\tau+d\tau-\kappa)} d\kappa + \psi_{\text{inf}}(\tau).
\end{aligned}
\tag{46}
$$

Because of the relation

$$
\int_0^{d\tau} \frac{A_{i\leftarrow j}(0,\tau+d\tau-\kappa;t+dt-\kappa)\psi_{\text{inf}}(\kappa-d\tau)}{I_j(0;t-\tau)\Psi_{\text{rec}}(\tau+d\tau-\kappa)} d\kappa \to 0,
\tag{47}
$$

Supplementary Eq. (46) can be written as

$$
\eta(\tau;t) = \int_0^{\tau} \frac{A_{i\leftarrow j}(0,\tau+d\tau-\kappa;t+dt-\kappa)\psi_{\text{inf}}(\kappa-d\tau)}{I_j(0;t-\tau)\Psi_{\text{rec}}(\tau+d\tau-\kappa)} d\kappa + \psi_{\text{inf}}(\tau).
\tag{48}
$$

Moreover, using the relations $\psi_{\text{inf}}(\kappa-d\tau) \to \psi_{\text{inf}}(\kappa)$ and $\Psi_{\text{rec}}(\tau+d\tau-\kappa) \to \Psi_{\text{rec}}(\tau-\kappa)$, we can rewrite Supplementary Eq. (48) as

$$
\eta(\tau;t) = \int_0^{\tau} \frac{A_{i\leftarrow j}(0,\tau+d\tau-\kappa;t+dt-\kappa)\psi_{\text{inf}}(\kappa)}{I_j(0;t-\tau)\Psi_{\text{rec}}(\tau-\kappa)} d\kappa + \psi_{\text{inf}}(\tau).
\tag{49}
$$

With the definition of $\eta(\tau;t)$ in Supplementary Eq. (45), we get

$$
\begin{aligned}
\eta(\tau;t) &= \int_0^{\tau} \eta(\tau-\kappa;t-\kappa)\psi_{\text{inf}}(\kappa)d\kappa + \psi_{\text{inf}}(\tau) \\
&= \int_0^{\tau} \eta(\kappa;t-\tau+\kappa)\psi_{\text{inf}}(\tau-\kappa)d\kappa + \psi_{\text{inf}}(\tau)
\end{aligned}
\tag{50}
$$

For $\forall t \geq 0$, we have

$$
\eta(0;t) = \psi_{\text{inf}}(0).
\tag{51}
$$

Solving the partial derivative of t for Supplementary Eq. (50), we get

$$
\eta_t'(\tau;t) = \int_0^{\tau} \eta_t'(\kappa;t-\tau+\kappa)\psi_{\text{inf}}(\tau-\kappa)d\kappa.
\tag{52}
$$

The partial derivative of t for $\eta(\tau;t)$ at $\tau = 0$ is thus zero:

$$
\eta_t'(0;t) = 0,
\tag{53}
$$

and $\eta_t'(0;t-\tau) = 0$. From Supplementary Eq. (52), we obtain the solution series: $\eta_t'(d\tau;t-\tau+d\tau) = 0$, $\eta_t'(2d\tau;t-\tau+2d\tau) = 0, \ldots, \eta_t'(\tau;t) = 0$. We thus have

$$
\forall t > 0, \forall \tau \leq t, \eta_t'(\tau;t) = 0,
\tag{54}
$$

where $\eta(\tau;t)$ is independent of t. Letting $\eta(\tau) = \eta(\tau;t)$, we rewrite Supplementary Eq. (50) as

$$
\eta(\tau) = \int_0^{\tau} \eta(\kappa)\psi_{\text{inf}}(\tau-\kappa)d\kappa + \psi_{\text{inf}}(\tau).
\tag{55}
$$

8

Performing Laplace transform on both sides of the equation, we obtain the following integral equation:

$$\eta(\tau) = \frac{1}{2\pi i} \int_{\sigma-i\infty}^{\sigma+i\infty} \frac{\hat{\psi}_{\mathrm{inf}}(s)}{1 - \hat{\psi}_{\mathrm{inf}}(s)} e^{s\tau} ds, \tag{56}$$

where [2]

$$\hat{\psi}_{\mathrm{inf}}(s) = \int_0^{+\infty} \psi_{\mathrm{inf}}(\tau) e^{-s\tau} d\tau. \tag{57}$$

Finally, Supplementary Eqs. (34), (36), (38) and (39) can be reduced to:

$$(\frac{\partial}{\partial\tau} + \frac{\partial}{\partial t}) I_i(\tau;t) = -\omega_{\mathrm{rec}}(\tau) I_i(\tau;t), \tag{58}$$

$$(\frac{\partial}{\partial\tau} + \frac{\partial}{\partial t}) S_i(\tau;t) = -S_i(\tau,t) \sum_{j=1}^{N} a_{ij} \Phi_{i\leftarrow j}(\tau;t), \tag{59}$$

$$I_i(0;t+dt) = \int_0^{+\infty} S_i(\tau;t) \sum_{j=1}^{N} a_{ij} \Phi_{i\leftarrow j}(\tau;t) d\tau, \tag{60}$$

$$S_i(0;t+dt) = \int_0^{+\infty} \omega_{\mathrm{rec}}(\tau) I_i(\tau;t) d\tau, \tag{61}$$

where

$$\Phi_{i\leftarrow j}(\tau;t) = \int_0^t \eta(\tau') I_i(\tau',t) d\tau'. \tag{62}$$

When the system reaches a steady state, we obtain the differential equations of probability density functions of node i being in the susceptible and infected states as

$$\frac{d\tilde{I}_i(\tau)}{d\tau} = -\omega_{\mathrm{rec}}(\tau) \tilde{I}_i(\tau), \tag{63}$$

$$\frac{d\tilde{S}_i(\tau)}{d\tau} = -\tilde{S}_i(\tau) \sum_{j=1}^{N} a_{ij} \int_0^{+\infty} \eta(\tau') \tilde{I}_j(\tau') d\tau', \tag{64}$$

and

$$\tilde{I}_i(0) = \tilde{S}_i(0). \tag{65}$$

Solving these equations, we obtain

$$\delta_{\mathrm{eff}} \tilde{I}_i = \frac{\tilde{S}_i}{\int_0^{+\infty} e^{-\delta_{\mathrm{eff}} \int_0^\tau \int_0^{+\infty} \eta(\tau') \Psi_{\mathrm{rec}}(\tau') d\tau' d\tau'' \sum_{j=1}^{N} a_{ij} \tilde{I}_j}}. \tag{66}$$

Defining

$$\lambda_{\mathrm{eff}} \equiv \int_0^{+\infty} \eta(\tau) \Psi_{\mathrm{rec}}(\tau) d\tau, \tag{67}$$

we can reduce the equation to

$$\tilde{I}_i = \lambda_{\mathrm{eff}} \tilde{S}_i \sum_{j=1}^{N} a_{ij} \tilde{I}_j, \tag{68}$$

9

Combining Supplementary Eq. (56) and the definition of λ_{eff}:

$$\lambda_{\text{eff}} \equiv \int_0^{+\infty} \Psi_{\text{rec}}(\tau) \frac{1}{2\pi i} \int_{\sigma-i\infty}^{\sigma+i\infty} \frac{\hat{\psi}_{\text{inf}}(s)}{1 - \hat{\psi}_{\text{inf}}(s)} e^{s\tau} d\tau ds, \tag{69}$$

and exchanging the integration order, we obtain

$$\lambda_{\text{eff}} = \frac{1}{2\pi i} \int_{\sigma-i\infty}^{\sigma+i\infty} \frac{\hat{\psi}_{\text{inf}}(s)[\hat{\psi}_{\text{rec}}(-s) - 1]}{1 - \hat{\psi}_{\text{inf}}(s)} \frac{ds}{s}, \tag{70}$$

where

$$\hat{\psi}_{\text{rec}}(s) = \int_0^{+\infty} \psi_{\text{rec}}(\tau) e^{-s\tau} d\tau. \tag{71}$$

Note that

$$\frac{1}{2\pi i} \int_{\sigma-i\infty}^{\sigma+i\infty} \frac{\hat{\psi}_{\text{inf}}(s)}{1 - \hat{\psi}_{\text{inf}}(s)} \frac{ds}{s} = 0, \tag{72}$$

when we take the integration path as a contour of an infinite radius, i.e., $s = re^{i\theta}$, where $r \to +\infty$, $-\frac{\pi}{2} < \theta < \frac{\pi}{2}$, and

$$\lim_{r \to +\infty} \frac{\hat{\psi}_{\text{inf}}(re^{i\theta})}{1 - \hat{\psi}_{\text{inf}}(re^{i\theta})} = 0. \tag{73}$$

We thus have

$$\lambda_{\text{eff}} = \frac{1}{2\pi i} \int_C \frac{\hat{\psi}_{\text{inf}}(s)\hat{\psi}_{\text{rec}}(-s)}{1 - \hat{\psi}_{\text{inf}}(s)} \frac{ds}{s}, \tag{74}$$

where C is a contour that encloses the entire $Re(s) > 0$ region [2].

SUPPLEMENTARY NOTE 3.   SECOND-ORDER MEAN FIELD THEORY AND ERROR ANALYSIS

A.   Second-order mean field theory

For SIS type of spreading dynamics, there are three distinct types of mean field theories, in the order of increase in the prediction accuracy and computational complexity: (1) the classical mean field theory based on the assumption that all nodes are equivalent [3], (2) heterogeneous mean field theory in which all the nodes with the same degree are assumed to be equivalent to each other [4], and (3) quench mean field theory where the state changes of individual nodes are treated separately [5, 6]. In these theories, the dynamical correlation between any pair of connected nodes is ignored, i.e., the states of any two connected nodes are regarded as independent. The three types of theories thus belong to first-order mean field analysis. To capture the dynamical correlation, a second-order approximation taking into account the evolution of the states of nodal pairs together is needed [7–13]. In fact, the pairwise approximation approach is a second-order theory, which regards nodal pairs with the same degree as equivalent [7–9, 13]. The master equation approach deals with not only the state changes of the nodes with the same degree, but also the state changes of their

neighbors. With approximations, it can be reduced to the evolution equations of pairwise approximation and mean field framework [14].

Here we develop a second-order mean field theory to deal with non-Markovian SIS dynamics. We first define the states of every pair of nodes. Specifically, for each pair of nodes, there are four different states: the $\langle II \rangle$ or $\langle AA \rangle$ state indicating that both nodes have been infected, the $\langle SI \rangle$ or $\langle SA \rangle$ state denoting that one node is susceptible and the other has been infected, the $\langle IS \rangle$ or $\langle AS \rangle$ state specifying that one node has been infected and the other is susceptible, and the $\langle SS \rangle$ state signifying that both nodes are susceptible. Note that the nodal pair states $\langle II \rangle$, $\langle SI \rangle$, $\langle IS \rangle$ are for type-I edge activation mechanism, and $\langle AA \rangle$, $\langle SA \rangle$, $\langle AS \rangle$ are for type-II edge activation mechanism.

The computational complexity required by the second-order mean field theory can often be prohibitively high. To make an analysis feasible, we restrict our study to the homogeneous case where the nodal pairs are equivalent in the Erdös-Rényi (ER) type of random networks. For type-I edge activation mechanism, we define $\langle II \rangle(\tau_1, \tau_2; t)$ as the probability density function that one node in a pair is in the infected state with the age of τ_1 and the other node is in the susceptible state with the age of τ_2 at time t. Similarly, the probabilities $\langle SI \rangle(\tau_1, \tau_2; t)$, $\langle IS \rangle(\tau_1, \tau_2; t)$, and $\langle SS \rangle(\tau_1, \tau_2; t)$ can be defined. The evolution equations of the pair node states for type-I activation are

$$(\frac{\partial}{\partial \tau} + \frac{\partial}{\partial t})I(\tau; t) = -\omega_{\mathrm{rec}}(\tau)I(\tau; t), \tag{75}$$

$$S(0; t + dt) = \int_0^{+\infty} \omega_{\mathrm{rec}}(\tau)I(\tau; t)d\tau, \tag{76}$$

$$(\frac{\partial}{\partial \tau} + \frac{\partial}{\partial t})S(\tau; t) = -S(\tau; t)\langle k \rangle \Phi(\tau; t), \tag{77}$$

$$I(0; t + dt) = \int_0^{+\infty} S(\tau; t)\langle k \rangle \Phi(\tau; t)d\tau, \tag{78}$$

$$(\frac{\partial}{\partial \tau_1} + \frac{\partial}{\partial \tau_2} + \frac{\partial}{\partial t})\langle II \rangle(\tau_1, \tau_2; t) = -[\omega_{\mathrm{rec}}(\tau_1) + \omega_{\mathrm{rec}}(\tau_2)]\langle II \rangle(\tau_1, \tau_2; t), \tag{79}$$

$$\langle SI \rangle(0, \tau_2; t) = \int_0^{+\infty} \omega_{\mathrm{rec}}(\tau_1)\langle II \rangle(\tau_1, \tau_2; t)d\tau_1, \tag{80}$$

$$\langle IS \rangle(\tau_1, 0; t) = \int_0^{+\infty} \omega_{\mathrm{rec}}(\tau_2)\langle II \rangle(\tau_1, \tau_2; t)d\tau_2, \tag{81}$$

$$(\frac{\partial}{\partial \tau_1} + \frac{\partial}{\partial \tau_2} + \frac{\partial}{\partial t})\langle SI \rangle(\tau_1, \tau_2; t)$$
$$= -\{(\langle k \rangle - 1)\Phi(\tau_1; t) + \omega_{\mathrm{inf}}[min(\tau_1, \tau_2)] + \omega_{\mathrm{rec}}(\tau_2)\}\langle SI \rangle(\tau_2, \tau_2; t), \tag{82}$$

$$\langle II \rangle(0, \tau_2; t) = \int_0^{+\infty} \{(\langle k \rangle - 1)\Phi(\tau_1; t) + \omega_{\mathrm{inf}}[min(\tau_1, \tau_2)]\}\langle SI \rangle(\tau_1, \tau_2; t)d\tau_1, \tag{83}$$

$$\langle SS \rangle(\tau_1, 0; t) = \int_0^{+\infty} \omega_{\mathrm{rec}}(\tau_2)\langle SI \rangle(\tau_1, \tau_2; t)d\tau_2, \tag{84}$$

$$(\frac{\partial}{\partial \tau_1} + \frac{\partial}{\partial \tau_2} + \frac{\partial}{\partial t})\langle IS \rangle(\tau_1, \tau_2; t)$$
$$= -\{\omega_{\mathrm{rec}}(\tau_1) + (\langle k \rangle - 1)\Phi(\tau_2; t) + \omega_{\mathrm{inf}}[min(\tau_1, \tau_2)]\}\langle SI \rangle(\tau_1, \tau_2; t), \tag{85}$$

11

$$\langle SS \rangle (0, \tau_2; t) = \int_0^{+\infty} \omega_{\text{rec}}(\tau_1) \langle IS \rangle (\tau_1, \tau_2; t) d\tau_1, \tag{86}$$

$$\langle II \rangle (\tau_1, 0; t) = \int_0^{+\infty} \{ (\langle k \rangle - 1) \Phi(\tau_2; t) + \omega_{\text{inf}}[min(\tau_1, \tau_2)] \} \langle IS \rangle (\tau_1, \tau_2; t) d\tau_2, \tag{87}$$

$$(\frac{\partial}{\partial \tau_1} + \frac{\partial}{\partial \tau_2} + \frac{\partial}{\partial t}) \langle SS \rangle (\tau_1, \tau_2; t)$$
$$= - [(\langle k \rangle - 1) \Phi(\tau_1; t) + (\langle k \rangle - 1) \Phi(\tau_2; t)] \langle SS \rangle (\tau_1, \tau_2; t), \tag{88}$$

$$\langle IS \rangle (0, \tau_2; t) = \int_0^{+\infty} (\langle k \rangle - 1) \Phi(\tau_1; t) \langle SS \rangle (\tau_1, \tau_2; t) d\tau_1, \tag{89}$$

$$\langle SI \rangle (\tau_1, 0; t) = \int_0^{+\infty} (\langle k \rangle - 1) \Phi(\tau_2; t) \langle SS \rangle (\tau_1, \tau_2; t) d\tau_2, \tag{90}$$

where

$$\Phi(\tau; t) = \int_0^{+\infty} \omega_{\text{inf}}[min(\tau, \tau_2)] \frac{\langle SI \rangle (\tau_1, \tau_2; t)}{S(\tau; t)} d\tau_2. \tag{91}$$

Equations (79)-(81) describe that, in the $\langle II \rangle$ nodal pair state, recovery of the infected node with age τ_1 converts the pair into the $\langle SI \rangle$ state, and the second node recovers to turn the pair into the $\langle IS \rangle$ state. Equations (82)-(84) represent that, in the $\langle SI \rangle$ state, infection of the susceptible node turns the nodal pair into the $\langle II \rangle$ state, while recovery of the infected node changes the pair into the $\langle SS \rangle$ state. Equations (85)-(87) dictate that, in $\langle IS \rangle$ nodal pair state, recovery of infected node switches the pair into the $\langle SS \rangle$ state while infection of the susceptible node converts the pair into the $\langle II \rangle$ state. Equations (88)-(90) indicate that, in the $\langle SS \rangle$ state, infection of the susceptible node with age τ_1 transforms the pair into the $\langle SI \rangle$ state, while infection of the susceptible node with age τ_2 converts the pair into the $\langle IS \rangle$ state.

For type-II edge activation mechanism, we define $\langle AA \rangle (\kappa_1, \tau_1, \kappa_2, \tau_2; t)$ as the probability density function that a directed edge from an infected node with age κ_1 to an infected node with age κ_2 is in the active state at age κ_1, while the inverted edge is in the active state with age κ_2. We define the probability density functions $\langle SA \rangle (\tau_1, \kappa_2, \tau_2; t)$, $\langle AS \rangle (\kappa_1, \tau_1, \tau_2; t)$, and $\langle SS \rangle (\tau_1, \tau_2; t)$ accordingly. The evolution equations of a nodal pair states can be written as

$$(\frac{\partial}{\partial \kappa} + \frac{\partial}{\partial \tau} + \frac{\partial}{\partial t}) A(\kappa, \tau; t) = -[\omega_{\text{inf}}(\kappa) + \omega_{\text{rec}}(\tau)] A(\kappa, \tau; t), \tag{92}$$

$$A(0, \tau + dt; t + dt) = \int_0^{+\infty} \omega_{\text{inf}}(\kappa) A(\kappa, \tau; t) d\kappa, \tag{93}$$

$$S(0; t + dt) = \int_0^{+\infty} \omega_{\text{rec}}(\tau) A(\kappa, \tau; t) d\tau, \tag{94}$$

$$(\frac{\partial}{\partial \tau} + \frac{\partial}{\partial t}) S(\tau; t) = -S(\tau; t) \langle k \rangle \Phi(\tau; t), \tag{95}$$

$$A(0, 0; t + dt) = \int_0^{+\infty} S(\tau; t) \langle k \rangle \Phi(\tau; t) d\tau, \tag{96}$$

$$(\frac{\partial}{\partial \kappa_1} + \frac{\partial}{\partial \tau_1} + \frac{\partial}{\partial \kappa_2} + \frac{\partial}{\partial \tau_2} + \frac{\partial}{\partial t}) \langle AA \rangle (\kappa_1, \tau_1, \kappa_2, \tau_2; t)$$
$$= - [\omega_{\text{inf}}(\kappa_1) + \omega_{\text{rec}}(\tau_1) + \omega_{\text{inf}}(\kappa_2) + \omega_{\text{rec}}(\tau_2)] \langle AA \rangle (\kappa_1, \tau_1, \kappa_2, \tau_2; t), \tag{97}$$

12

$$\langle AA\rangle(0,\tau_1,\kappa_2,\tau_2;t)=\int_0^{+\infty}\omega_{\text{inf}}(\kappa_1)\langle AA\rangle(\kappa_1,\tau_1,\kappa_2,\tau_2;t)d\kappa_1, \tag{98}$$

$$\langle SA\rangle(0,\kappa_2,\tau_2;t)=\int_0^{+\infty}\omega_{\text{rec}}(\tau_1)\langle AA\rangle(\kappa_1,\tau_1,\kappa_2,\tau_2;t)d\tau_1, \tag{99}$$

$$\langle AA\rangle(\kappa_1,\tau_1,0,\tau_2;t)=\int_0^{+\infty}\omega_{\text{inf}}(\kappa_2)\langle AA\rangle(\kappa_1,\tau_1,\kappa_2,\tau_2;t)d\kappa_2, \tag{100}$$

$$\langle AS\rangle(\kappa_1,\tau_1,0;t)=\int_0^{+\infty}\omega_{\text{rec}}(\tau_2)\langle AA\rangle(\kappa_1,\tau_1,\kappa_2,\tau_2;t)d\tau_2, \tag{101}$$

$$(\frac{\partial}{\partial\tau_1}+\frac{\partial}{\partial\kappa_2}+\frac{\partial}{\partial\tau_2}+\frac{\partial}{\partial t})\langle SA\rangle(\tau_1,\kappa_2,\tau_2;t)$$
$$=-\{(\langle k\rangle-1)\Phi(\tau_1;t)+\omega_{\text{inf}}(\kappa_2)+\omega_{\text{rec}}(\tau_2)\}\langle SA\rangle(\tau_1,\kappa_2,\tau_2;t), \tag{102}$$

$$\langle AA\rangle(0,0,\kappa_2,\tau_2;t)=\int_0^{+\infty}(\langle k\rangle-1)\Phi(\tau_1;t)\langle SA\rangle(\tau_1,\kappa_2,\tau_2;t)d\tau_1, \tag{103}$$

$$\langle AA\rangle(0,0,0,\tau_2;t)=\int_0^{+\infty}\omega_{\text{inf}}(\kappa_2)\langle SA\rangle(\tau_1,\kappa_2,\tau_2;t)d\kappa_2, \tag{104}$$

$$\langle SS\rangle(\tau_1,0;t)=\int_0^{+\infty}\int_0^{+\tau_2}\omega_{\text{rec}}(\tau_2)\langle SA\rangle(\tau_1,\kappa_2,\tau_2;t)d\kappa_2 d\tau_2, \tag{105}$$

$$(\frac{\partial}{\partial\kappa_1}+\frac{\partial}{\partial\tau_1}+\frac{\partial}{\partial\tau_2}+\frac{\partial}{\partial t})\langle AS\rangle(\kappa_1,\tau_1,\tau_2;t)$$
$$=-\{\omega_{\text{inf}}(\kappa_2)+\omega_{\text{rec}}(\tau_1)+(\langle k\rangle-1)\Phi(\tau_2;t)\}\langle AS\rangle(\kappa_1,\tau_1,\tau_2;t), \tag{106}$$

$$\langle AA\rangle(0,\tau_1,0,0;t)=\int_0^{+\infty}\omega_{\text{inf}}(\kappa_1)\langle AS\rangle(\kappa_1,\tau_1,\tau_2;t)d\kappa_1, \tag{107}$$

$$\langle SS\rangle(0,\tau_2;t)=\int_0^{+\infty}\int_0^{+\tau_1}\omega_{\text{rec}}(\tau_1)\langle AS\rangle(\kappa_1,\tau_1,\tau_2;t)d\kappa_1 d\tau_1, \tag{108}$$

$$\langle AA\rangle(\kappa_1,\tau_1,0,0;t)=\int_0^{+\infty}(\langle k\rangle-1)\Phi(\tau_2;t)\langle AS\rangle(\kappa_1,\tau_1,\tau_2;t)d\tau_2, \tag{109}$$

$$(\frac{\partial}{\partial\tau_1}+\frac{\partial}{\partial\tau_2}+\frac{\partial}{\partial t})\langle SS\rangle(\tau_1,\tau_2;t)$$
$$=-[(\langle k\rangle-1)\Phi(\tau_1;t)+(\langle k\rangle-1)\Phi(\tau_2;t)]\langle SS\rangle(\tau_1,\tau_2;t), \tag{110}$$

$$\langle AS\rangle(0,0,\tau_2;t)=\int_0^{+\infty}(\langle k\rangle-1)\Phi(\tau_1;t)\langle SS\rangle(\tau_1,\tau_2;t)\tau_1, \tag{111}$$

$$\langle SA\rangle(\tau_1,0,0;t)=\int_0^{+\infty}(\langle k\rangle-1)\Phi(\tau_2;t)\langle SS\rangle(\tau_1,\tau_2;t)\tau_2, \tag{112}$$

where

$$\Phi(\tau;t)=\int_0^{+\infty}\int_0^{+\tau_2}\omega_{\text{inf}}(\kappa_2)\frac{\langle SA\rangle(\tau_1,\kappa_2,\tau_2;t)}{S(\tau;t)}d\kappa_2 d\tau_2. \tag{113}$$

Equations (98)-(101), respectively, describe that in the $\langle AA\rangle$ nodal pair state, disease transmission from an infected node with age τ_1 and directed edge age κ_1 to an infected node of age τ_2 and directed edge age κ_2 converts the nodal pair into the $\langle AA\rangle$ state with $\kappa_1=0$, the recovery of an infected node with age τ_1 transforms the pair into the $\langle SA\rangle$ state, disease transmission from the infected node with age τ_2 and directed edge age κ_2 to the infected

13

node of age τ_1 and directed edge age κ_1 turns the pair into the $\langle AA \rangle$ state with $\kappa_2 = 0$, and the recovery of the infected node with age τ_2 places the pair into the $\langle AS \rangle$ state. Similarly, Supplementary Eqs. (102)-(105), respectively, indicate that in the $\langle SA \rangle$ state, the susceptible node is infected by its neighbors other than the infected node aged at τ_2 so that the pair is turned into the $\langle AA \rangle$ state, the susceptible node is infected by the infected node of τ_2 and so the pair gets into the $\langle AA \rangle$ state, and recovery of the infected node aged at τ_2 places the pair into the $\langle SS \rangle$ state. Equations (106)-(109) indicate, respectively, that in the $\langle AS \rangle$ state, disease transmission from an infected node with age τ_1 and directed edge age κ_1 to a susceptible node of age τ_2 changes the pair into the $\langle AA \rangle$ state, recovery of the infected node with age τ_1 transforms the pair into the $\langle SS \rangle$ state, and the susceptible node is infected by its neighbors other than the infected node and thus the nodal pair transitions into the $\langle AA \rangle$ state. Equations (110), (111), and (112) mean, respectively, that for the $\langle SS \rangle$ state pair, the susceptible node aged at τ_1 is infected and thus the pair moves into the $\langle AS \rangle$ state, and the susceptible node aged at τ_2 is infected and so the pair changes into the $\langle SA \rangle$ state.

To verify the accuracy of the second-order mean field theory, we set the infection time and recovery time distributions to be the Weibullean type. Supplementary Fig. 2 shows that the theory is capable of predicting the simulation results more accurately than the first-order theory for ER random networks, even for the situation where the disease has a high decay rate [e.g., $\alpha_I = 4$ in Supplementary Figs. 2(c) and 2(d)].

B.   Error Analysis

Our development of the second-order theory, due to its relatively high accuracy, enables an analysis of the source of errors in the first-order mean field theory through a comparison between the results from the first-order and the second-order theories. (For a network with N nodes, the most accurate description is the Nth-order mean field theory, but it is practically infeasible to analyze theories with order higher than two.) Because the dynamical correlation between any nodal pair is completely ignored in the first-order theory, the error analysis enables an understanding of the effects of dynamical correlation on non-Markovian dynamics with respect to different edge activation mechanisms.

To begin a systematic error analysis, we rewrite the relevant equations from the first-order theory in a similar form to those in the second-order theory. Recall that the assumptions employed in the first-order theory, which are

$$\langle II \rangle(\tau_1, \tau_2; t) = I(\tau_1; t)I(\tau_2; t), \tag{114}$$

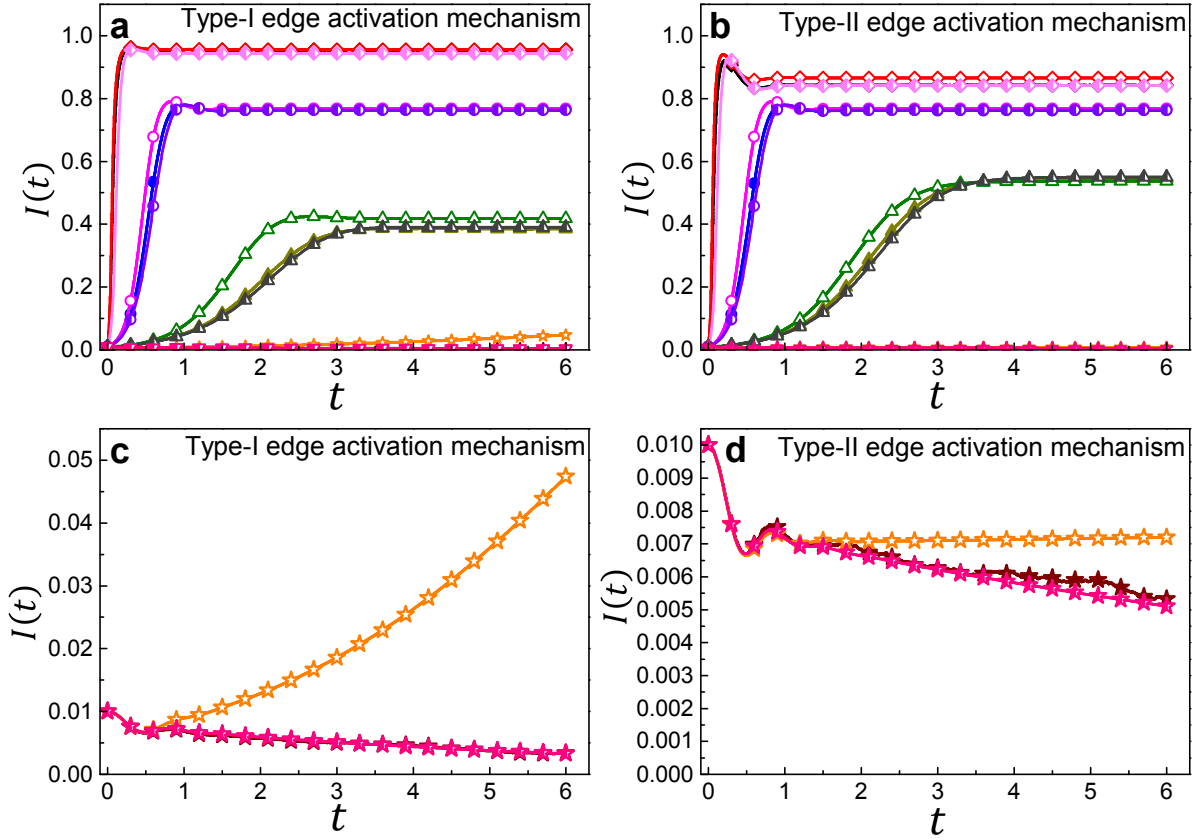$$\langle SI \rangle(\tau_1, \tau_2; t) = S(\tau_1; t)I(\tau_2; t), \tag{115}$$

$$\langle IS \rangle(\tau_1, \tau_2; t) = I(\tau_1; t)S(\tau_2; t), \tag{116}$$

$$\langle SS \rangle(\tau_1, \tau_2; t) = S(\tau_1; t)S(\tau_2; t), \tag{117}$$

$$\langle AA \rangle(\kappa_1, \tau_1, \kappa_2, \tau_2; t) = A(\kappa_1, \tau_1; t)A(\kappa_2, \tau_2; t), \tag{118}$$

$$\langle SA \rangle(\tau_1, \kappa_2, \tau_2; t) = S(\tau_1; t)A(\kappa_2, \tau_2; t), \tag{119}$$

$$\langle AS \rangle(\kappa_1, \tau_1, \tau_2; t) = A(\kappa_1, \tau_1; t)S(\tau_2; t). \tag{120}$$

14

Supplementary Figure 2. Comparison of time evolution between simulated and theoretical results. **a**,**b** Time evolution for type-I and type-II mechanism, respectively. **c**,**d** Extinction process with $\alpha_{\mathrm{I}} = 4$ for type-I and type-II mechanism, respectively. In all panels, the solid symbols represent the simulation results averaged over 100 realizations on ER random networks, the open symbols represent the results of theoretical solutions obtained from the first-order mean field theory, and the half solid symbols correspond to the theoretical results from Supplementary Eqs. (75)-(113) in the second-order theory. Diamonds, circles, triangles, and stars are for $\alpha_{\mathrm{I}} = 0.5, 1, 2, 4$, respectively. The random networks have size $N = 10^4$ and mean degree $\langle k \rangle \approx 10$. Other parameters are $\beta_{\mathrm{I}} = 1$, $\alpha_{\mathrm{R}} = 2$, and $\beta_{\mathrm{R}} = 0.5$.

For $\langle SI \rangle(\tau_1, \tau_2; t)$, we can obtain its evolution equation as

$$
\begin{aligned}
&(\frac{\partial}{\partial \tau_1} + \frac{\partial}{\partial \tau_2} + \frac{\partial}{\partial t})[S(\tau_1; t)I(\tau_2; t)] \\
&= \frac{S(\tau_1 + dt; t + dt)I(\tau_2 + dt; t + dt) - S(\tau_1; t)I(\tau_2; t)}{dt} \\
&= S(\tau_1 + dt; t + dt)\frac{I(\tau_2 + dt; t + dt) - I(\tau_2; t)}{dt} + I(\tau_2; t)\frac{S(\tau_1 + dt; t + dt) - S(\tau_1; t)}{dt} \quad (121) \\
&= S(\tau_1; t)(\frac{\partial}{\partial \tau_1} + \frac{\partial}{\partial t})I(\tau_2; t) + I(\tau_2; t)(\frac{\partial}{\partial \tau_1} + \frac{\partial}{\partial t})S(\tau_1; t) \\
&= -[\Phi(\tau_1; t) + \omega_{\mathrm{rec}}(\tau_2)]S(\tau_1; t)I(\tau_2; t),
\end{aligned}
$$

$$I(0;t)I(\tau_2;t) = I(\tau_2;t)\int_0^{+\infty} \langle k \rangle S(\tau_1)d\tau_1 = \int_0^{+\infty} \langle k \rangle S(\tau_1)I(\tau_2;t)d\tau_1, \tag{122}$$

$$S(\tau_1;t)S(0;t) = S(\tau_1;t)\int_0^{+\infty} \omega_{\mathrm{rec}}(\tau_2)I(\tau_2)d\tau_2 = \int_0^{+\infty} \omega_{\mathrm{rec}}(\tau_2)S(\tau_1;t)I(\tau_2)d\tau_2. \tag{123}$$

For type-I edge activation mechanism, we can get another form of the first-order mean field theory as

$$(\frac{\partial}{\partial \tau_1} + \frac{\partial}{\partial \tau_2} + \frac{\partial}{\partial t})\langle II \rangle(\tau_1, \tau_2; t) = -[\omega_{\mathrm{rec}}(\tau_1) + \omega_{\mathrm{rec}}(\tau_2)]\langle II \rangle(\tau_1, \tau_2; t), \tag{124}$$

$$\langle SI \rangle(0, \tau_2; t) = \int_0^{+\infty} \omega_{\mathrm{rec}}(\tau_1)\langle II \rangle(\tau_1, \tau_2; t)d\tau_1, \tag{125}$$

$$\langle IS \rangle(\tau_1, 0; t) = \int_0^{+\infty} \omega_{\mathrm{rec}}(\tau_2)\langle II \rangle(\tau_1, \tau_2; t)d\tau_2, \tag{126}$$

$$(\frac{\partial}{\partial \tau_1} + \frac{\partial}{\partial \tau_2} + \frac{\partial}{\partial t})\langle SI \rangle(\tau_1, \tau_2; t)$$
$$= -[\langle k \rangle \Phi(\tau_1; t) + \omega_{\mathrm{rec}}(\tau_2)]\langle SI \rangle(\tau_2, \tau_2; t), \tag{127}$$

$$\langle II \rangle(0, \tau_2; t) = \int_0^{+\infty} \langle k \rangle \Phi(\tau_1; t)\langle SI \rangle(\tau_1, \tau_2; t)\tau_1, \tag{128}$$

$$\langle SS \rangle(\tau_1, 0; t) = \int_0^{+\infty} \omega_{\mathrm{rec}}(\tau_2)\langle SI \rangle(\tau_1, \tau_2; t)\tau_2, \tag{129}$$

$$(\frac{\partial}{\partial \tau_1} + \frac{\partial}{\partial \tau_2} + \frac{\partial}{\partial t})\langle IS \rangle(\tau_1, \tau_2; t)$$
$$= -[\omega_{\mathrm{rec}}(\tau_1) + \langle k \rangle \Phi(\tau_2; t)]\langle IS \rangle(\tau_1, \tau_2; t), \tag{130}$$

$$\langle SS \rangle(0, \tau_2; t) = \int_0^{+\infty} \omega_{\mathrm{rec}}(\tau_1)\langle IS \rangle(\tau_1, \tau_2; t)\tau_1, \tag{131}$$

$$\langle II \rangle(\tau_1, 0; t) = \int_0^{+\infty} \langle k \rangle \Phi(\tau_2; t)\langle IS \rangle(\tau_1, \tau_2; t)d\tau_2, \tag{132}$$

$$(\frac{\partial}{\partial \tau_1} + \frac{\partial}{\partial \tau_2} + \frac{\partial}{\partial t})\langle SS \rangle(\tau_1, \tau_2; t)$$
$$= -[\langle k \rangle \Phi(\tau_1; t) + \langle k \rangle \Phi(\tau_2; t)]\langle SS \rangle(\tau_1, \tau_2; t), \tag{133}$$

$$\langle IS \rangle(0, \tau_2; t) = \int_0^{+\infty} \langle k \rangle \Phi(\tau_1; t)\langle SS \rangle(\tau_1, \tau_2; t)d\tau_1, \tag{134}$$

$$\langle SI \rangle(\tau_1, 0; t) = \int_0^{+\infty} \langle k \rangle \Phi(\tau_2; t)\langle SS \rangle(\tau_1, \tau_2; t)d\tau_2, \tag{135}$$

where

$$\Phi(\tau; t) = \int_0^{+\infty} \omega_{\mathrm{inf}}[\min(\tau, \tau_2)]\frac{\langle SI \rangle(\tau_1, \tau_2; t)}{S(\tau; t)}d\tau_2$$
$$= \int_0^{+\infty} \omega_{\mathrm{inf}}[\min(\tau, \tau_2)]I(\tau_2; t)d\tau_2. \tag{136}$$

16

For type-II edge activation mechanism, we have

$$
(\frac{\partial}{\partial \kappa_1} + \frac{\partial}{\partial \tau_1} + \frac{\partial}{\partial \kappa_2} + \frac{\partial}{\partial \tau_2} + \frac{\partial}{\partial t})\langle AA \rangle(\kappa_1, \tau_1, \kappa_2, \tau_2; t) \tag{137}
$$
$$
= -[\omega_{\inf}(\kappa_1) + \omega_{\rec}(\tau_1) + \omega_{\inf}(\kappa_2) + \omega_{\rec}(\tau_2)]\langle AA \rangle(\kappa_1, \tau_1, \kappa_2, \tau_2; t),
$$

$$
\langle AA \rangle(0, \tau_1, \kappa_2, \tau_2; t) = \int_0^{+\infty} \omega_{\inf}(\kappa_1)\langle AA \rangle(\kappa_1, \tau_1, \kappa_2, \tau_2; t)d\kappa_1, \tag{138}
$$

$$
\langle SA \rangle(0, \kappa_2, \tau_2; t) = \int_0^{+\infty} \omega_{\rec}(\tau_1)\langle AA \rangle(\kappa_1, \tau_1, \kappa_2, \tau_2; t)d\tau_1, \tag{139}
$$

$$
\langle AA \rangle(\kappa_1, \tau_1, 0, \tau_2; t) = \int_0^{+\infty} \omega_{\inf}(\kappa_2)\langle AA \rangle(\kappa_1, \tau_1, \kappa_2, \tau_2; t)d\kappa_2, \tag{140}
$$

$$
\langle AS \rangle(\kappa_1, \tau_1, 0; t) = \int_0^{+\infty} \omega_{\rec}(\tau_2)\langle AA \rangle(\kappa_1, \tau_1, \kappa_2, \tau_2; t)d\tau_2, \tag{141}
$$

$$
(\frac{\partial}{\partial \tau_1} + \frac{\partial}{\partial \kappa_2} + \frac{\partial}{\partial \tau_2} + \frac{\partial}{\partial t})\langle SA \rangle(\tau_1, \kappa_2, \tau_2; t) \tag{142}
$$
$$
= -\{\langle k \rangle \Phi(\tau_1; t) + \omega_{\inf}(\kappa_2) + \omega_{\rec}(\tau_2)\}\langle SA \rangle(\tau_1, \kappa_2, \tau_2; t),
$$

$$
\langle AA \rangle(0, 0, \kappa_2, \tau_2; t) = \int_0^{+\infty} \langle k \rangle \Phi(\tau_1; t)\langle SA \rangle(\tau_1, \kappa_2, \tau_2; t)d\tau_1, \tag{143}
$$

$$
\langle SA \rangle(\kappa_1, \tau_1, 0, \tau_2; t) = \int_0^{+\infty} \omega_{\inf}(\kappa_2)\langle SA \rangle(\tau_1, \kappa_2, \tau_2; t)d\kappa_2, \tag{144}
$$

$$
\langle SS \rangle(\tau_1, 0; t) = \int_0^{+\infty} \int_0^{+\tau_2} \omega_{\rec}(\tau_2)\langle SA \rangle(\tau_1, \kappa_2, \tau_2; t)d\kappa_2 d\tau_2, \tag{145}
$$

$$
(\frac{\partial}{\partial \kappa_1} + \frac{\partial}{\partial \tau_1} + \frac{\partial}{\partial \tau_2} + \frac{\partial}{\partial t})\langle AS \rangle(\kappa_1, \tau_1, \tau_2; t) \tag{146}
$$
$$
= -\{\omega_{\inf}(\kappa_2) + \omega_{\rec}(\tau_1) + \langle k \rangle \Phi(\tau_2; t)\}\langle AS \rangle(\kappa_1, \tau_1, \tau_2; t),
$$

$$
\langle AS \rangle(0, \tau_2, \kappa_2, \tau_2; t) = \int_0^{+\infty} \omega_{\inf}(\kappa_1)\langle AS \rangle(\kappa_1, \tau_1, \tau_2; t)d\kappa_1, \tag{147}
$$

$$
\langle SS \rangle_{(}0, \tau_2; t) = \int_0^{+\infty} \int_0^{+\tau_1} \omega_{\rec}(\tau_1)\langle AS \rangle(\kappa_1, \tau_1, \tau_2; t)d\kappa_1 d\tau_1, \tag{148}
$$

$$
\langle AA \rangle(\kappa_1, \tau_1, 0, 0; t) = \int_0^{+\infty} \langle k \rangle \Phi(\tau_2; t)\langle AS \rangle(\kappa_1, \tau_1, \tau_2; t)d\tau_2, \tag{149}
$$

$$
(\frac{\partial}{\partial \tau_1} + \frac{\partial}{\partial \tau_2} + \frac{\partial}{\partial t})\langle SS \rangle(\tau_1, \tau_2; t) \tag{150}
$$
$$
= -[\langle k \rangle \Phi(\tau_1; t) + \langle k \rangle \Phi(\tau_2; t)]\langle SS \rangle(\tau_1, \tau_2; t),
$$

$$
\langle AS \rangle(0, 0, \tau_2; t) = \int_0^{+\infty} \langle k \rangle \Phi(\tau_1; t)\langle SS \rangle(\tau_1, \tau_2; t)\tau_1, \tag{151}
$$

$$
\langle SA \rangle(\tau_1, 0, 0; t) = \int_0^{+\infty} \langle k \rangle \Phi(\tau_2; t)\langle SS \rangle(\tau_1, \tau_2; t)\tau_2, \tag{152}
$$

17

where

$$
\begin{aligned}
\Phi(\tau; t) &= \int_0^{+\infty} \int_0^{+\tau_2} \omega_{\text{inf}}(\kappa_2) \frac{\langle SA \rangle(\tau_1, \kappa_2, \tau_2; t)}{S(\tau; t)} d\kappa_2 d\tau_2 \\
&= \int_0^{+\infty} \int_0^{+\tau_2} \omega_{\text{inf}}(\kappa_2) A(\kappa_2, \tau_2; t) d\kappa_2 d\tau_2.
\end{aligned}
\tag{153}
$$

For type-I edge activation mechanism, we compare Supplementary Eqs. (79)-(81) with Supplementary Eqs. (124)-(126) to assess the dynamical correlation of the $\langle II \rangle$ state. We find that the two groups of equations are essentially identical, so there is no dynamical correlation between two infected nodes. Comparing Supplementary Eqs. (82) and (83), we see that, in Supplementary Eqs. (127) and (128) $\omega_{\text{inf}}[\min(\tau_1, \tau_2)]$ is replaced by $\Phi(\tau_1; t)$, indicating that the first-order mean field theory ignores any temporal correlation between an infected node and a susceptible node, enlarging the bias in describing the $\langle SI \rangle$ state. For the $\langle IS \rangle$ state, the method of analysis is the same as that for the $\langle SI \rangle$ state. For the $\langle SS \rangle$ state, we compare Supplementary Eqs. (88)-(90) with Supplementary Eqs. (133)-(135) and find that the quantity $\langle k \rangle - 1$ is replaced by $\langle k \rangle$. This means that the first-order mean field theory attempts to include the non-existent process of infection between two susceptible nodes, which is another source of error.

For type-II edge activation mechanism, we compare Supplementary Eqs. (97)-(101) with Supplementary Eqs. (137)-(141) to assess the dynamical correlation of the $\langle AA \rangle$ state. Note that the two groups of equations are identical, so there is no dynamical correlation between any pair of infected nodes. For the $\langle SA \rangle$ state, we compare Supplementary Eqs. (102)-(103) with Supplementary Eqs. (142)-(143) and identify the simple replacement of $\langle k \rangle - 1$ by $\langle k \rangle$. In addition, the quantity $\langle AA \rangle(0, 0, 0, \tau_2; t)$ in Supplementary Eq. (144) is replaced by $\langle SA \rangle(\kappa_1, \tau_1, 0, \tau_2; t)$ in Supplementary Eq. (104). In the first-order equations, the infection of a susceptible node from any of its neighbors and the disease transmission through the active edge are considered as two independent processes. Specifically, the susceptible node would be infected by all its neighbors including the infected node [see Supplementary Eq. (143)], but disease transmission through such an active edge cannot result in the infection of the susceptible node [see Supplementary Eq. (144)]. This means that the first-order mean field theory ignores the causality between disease transmission through an active edge and infection of the susceptible node. For the $\langle SS \rangle$ state, we compare Supplementary Eqs. (110)-(112) with Supplementary Eqs. (150)-(152), and find that $\langle k \rangle - 1$ in the latter is replaced by $\langle k \rangle$ in the former, which means that the first-order mean field erroneously takes into account the non-existent infection process between two susceptible nodes.

The error analysis indicates that the two activation rules have distinct effects of dynamical correlation on active edges. For type-I edge activation mechanism, the errors in the first-order mean field theory mainly result from the temporal correlations on active edges, while for type-II edge activation mechanism, the errors are caused by the causality between disease transmission through the active edge and infection of the susceptible node.

18
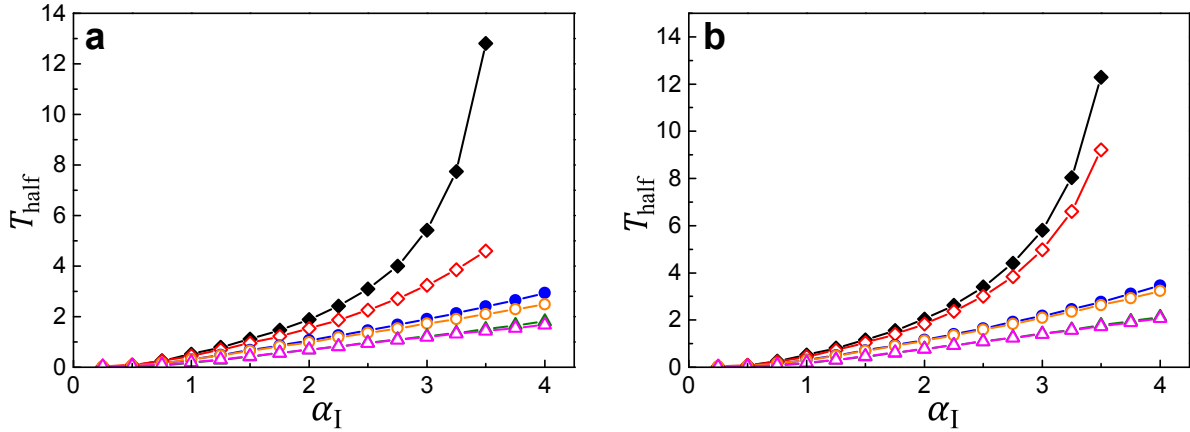
Supplementary Figure 3. Transient time versus α_{I}. The extent of the infection time distribution is characterized by α_{I}, where a smaller value of α_{I} corresponds to a narrower distribution. Panels **a-b** are for results from the SIS model with type-I activation and type-II activation mechanisms, respectively. The solid and open symbols represent simulation and theoretical results, respectively. Diamonds, circles, and triangles, respectively, are for random, scale-free and Hamsterster networks.

SUPPLEMENTARY NOTE 4.   EFFECT OF INFECTION TIME DISTRIBUTION ON TRANSIENT TIME

The effect of the inter-event time distribution on the speed of spreading dynamics is an issue of interest [15–19]. Because the time that the system has reached a steady state cannot be sharply defined, we set the empirical rule to determine the transient time T_{half} as the time at which the infected density reaches the average value between the initial density $I(0)$ and the steady-state density $\tilde{I}$. Supplementary Fig. 3 shows that a narrower distribution of the inter-event times, which corresponds to a smaller value of α_{I}, makes it easier for the system to reach a final steady state.

SUPPLEMENTARY NOTE 5.   EFFECT OF DEGREE DISTRIBUTION ON TRANSIENT TIME

In general, the network topology can affect the spreading speed as well [20–25]. To address this issue, we investigate the relationship between transient lifetime and the degree distribution. To be concrete, we study the transient time on scale-free networks constructed from the uncorrelated configuration model [28]. Supplementary Fig. 4(a) shows that a smaller value of the power-law degree exponent γ enables the spreading dynamics to reach its steady state faster. The lower-cutoff degree D_{low} of the degree distribution can also affect the transient lifetime, as shown in Supplementary Fig. 4(b), where a larger value of D_{low} can also expedite the spreading dynamics in approaching the final steady state. These results indicate that effects of degree distribution on transient time for non-Markovian spreading dynamics are consistent with those for Markovian dynamics.
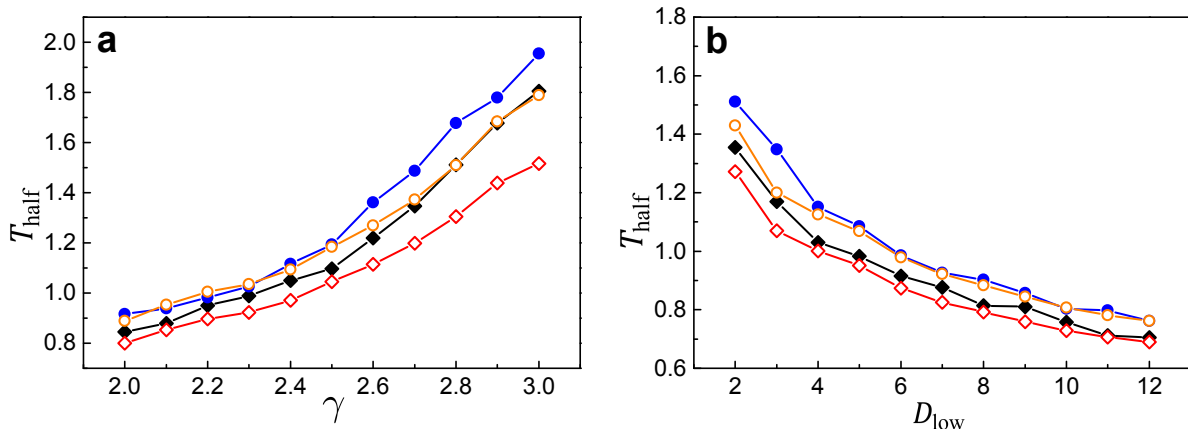
Supplementary Figure 4. Effect of network degree distribution on transient lifetime. Shown is the transient time versus two specific network structural parameter: power-law degree exponent γ and lower-cutoff degree D_{low}. In general, a smaller value of γ corresponds to the network with more hub nodes. **a-b** Results for SIS dynamics with respect to γ and D_{low}, respectively. The solid and open symbols represent simulation and theoretical results, respectively. Diamonds and circles are for type-I and type-II activation, respectively. In **a**, the value of D_{low} is fixed at five, while that of γ is set to be 2.3 in panel **b**. The networks have size $N = 10^4$ and the structural cutoff is characterized by the maximum degree $k_{max} \sim N^{1/2}$. Other parameters are $\alpha_{\text{I}} = 2$, $\beta_{\text{I}} = 1$, $\alpha_{\text{R}} = 2$, and $\beta_{\text{R}} = 0.5$.
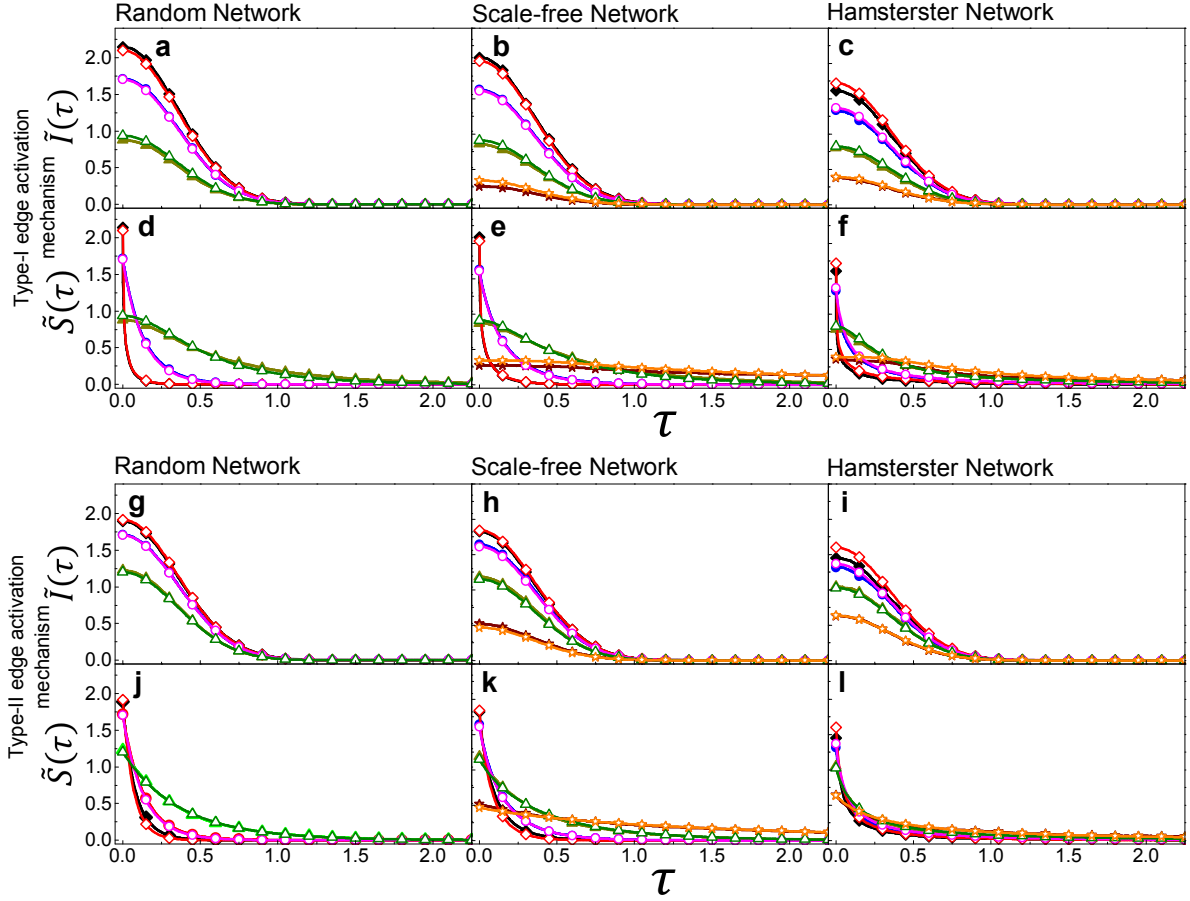
SUPPLEMENTARY NOTE 6. STATIONARY PROBABILITY DENSITY DISTRIBUTIONS

To validate our proposed first-order mean field theory for non-Markovian processes, we examine the stationary probability density functions $\tilde{I}(\tau)$ and $\tilde{S}(\tau)$ defined as

$$\tilde{I}(\tau) = \frac{\sum_{i=1}^{N} \tilde{I}_i(\tau)}{N}, \tag{154}$$

$$\tilde{S}(\tau) = \frac{\sum_{i=1}^{N} \tilde{S}_i(\tau)}{N}, \tag{155}$$

and compare the theoretical predictions with the simulation results in Supplementary Fig. 5. Especially, we count the numbers of infected and susceptible nodes at every discrete state age (at the age difference $\Delta\tau = 0.001$) when the system reaches a steady state, and divide the numbers by $\Delta\tau \times N$ to get the simulated stationary probability density. The theoretical predictions agree with the simulation results for random, scale-free, and Hamsterster networks. The difference between SIS models with type-I and type-II edge activation mechanisms is that the results of $\tilde{S}(\tau)$ for the former decrease more smoothly than the latter in the region of small τ values for $\alpha_{\text{I}} = 2, 4$, indicating that newly recovered nodes in the latter are more susceptible to infection than the ones in the former. For $\alpha_{\text{I}} = 2, 4$, the infection rate increases with the age of the active edge. By type-II edge activation mechanism, the ages of the active edges depend only on the infected nodes and thus may be greater than those in type-I edge activation, resulting in some greater infection rate.

Supplementary Figure 5. Comparison of stationary probability density distributions between simulated and theoretical results. Panels in the first two rows show the results from the SIS model with type-I activation mechanism, and those in the last two rows present the results for the model with type-II mechanism. Panels in the first and third rows present the results of $\tilde{I}(\tau)$ while those in the second and fourth rows demonstrate the results of $\tilde{S}(\tau)$. Panels in the three columns (from left to right) are simulated or solved from theoretically derived evolution equations for random, scale-free and Hamsterster networks, respectively. The solid and open symbols represent simulation and theoretical results, respectively. Diamonds, circles, triangles, and stars, respectively, correspond to $\alpha_I = 0.5, 1, 2, 4$. The random and scale-free networks have size $N = 10^4$ and mean degree $\langle k \rangle \approx 10$, and the Hamsterster network parameters are $N = 2426$ and $\langle k \rangle \approx 13.7$. Other parameters are $\beta_I = 1$, $\alpha_R = 2$, and $\beta_R = 0.5$. Note that the lack of data points in the random network for $\alpha_I = 4$ is due to the extinction of the infected density.

SUPPLEMENTARY NOTE 7.   SPECIAL CASE I: MARKOVIAN EQUIVALENCE OF NON-MARKOVIAN SIS MODEL WITH TYPE-I EDGE ACTIVATION MECHANISM

For $\alpha_I = 1$, the Weibull distribution reduces to an exponential distribution. In this case, the non-Markovian SIS with type-I activation mechanism is completely equivalent to
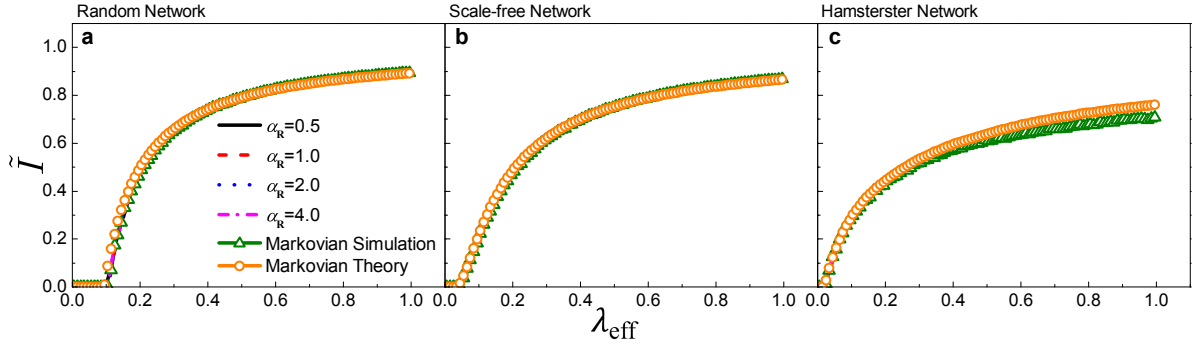
Supplementary Figure 6. Comparison of stationary infected density with type-I edge activation mechanism. Panels **a-c** are for results from random, scale-free, and Hamsterster networks, respectively. Solid, dashed, dotted, and dot-dashed curves, respectively, represent the results for $\alpha_R = 0.5, 1, 2, 4$. Triangles and circles correspond to results from the Markovian process and the analytical solution, respectively. Other parameters are $\alpha_I = 1$ and $\beta_R = 0.5$.

a Markovian SIS process. We set

$$\psi_{\text{inf}}(\kappa) = \frac{1}{\beta_I}e^{-\frac{\kappa}{\beta_I}}, \tag{156}$$

$$\psi_{\text{rec}}(\tau) = \frac{\alpha_R}{\beta_R}(\frac{\tau}{\beta_R})^{\alpha_R-1}e^{-(\frac{\tau}{\beta_R})^{\alpha_R}}. \tag{157}$$

For $\alpha_R = \{0.5, 1, 2, 4\}$ and $\beta_R = 0.5$, we adjust the value of λ_{eff} through changing β_I, where

$$\lambda_{\text{eff}} = \frac{\beta_R\Gamma(1/\alpha_R)}{\alpha_R\beta_I}, \tag{158}$$

and Γ is the gamma function. In Supplementary Figs. 6(a,b), we present results from Monte Carlo simulations for the three types of networks. The theoretical results from the Markovian process are obtained from a first-order mean field analysis. For all values of λ_{eff} (or β_I), there is a good agreement between the infected density for $\alpha_I = 1$ with the theoretical prediction of the Markovian model.

SUPPLEMENTARY NOTE 8.   SPECIAL CASE II: NON-MARKOVIAN SPREADING ON STRONG HETEROGENEOUS NETWORKS

We test our theory on scale-free networks with a strong heterogeneous degree distribution, where the values of the network parameters are: size 10000, power-law degree exponent 2.3, lower cutoff degree being five, upper cutoff degree being about 100, and average degree approximately 11.9. A network in this ensemble has a large number of hub nodes. As shown in Supplementary Fig. 7, even in this relatively extreme case, our theory is able to predict the simulation results. Furthermore, when the spreading has reached the steady state, the approximate equivalence between non-Markovian and Markovian dynamics for both type-I and type-II activation mechanisms holds.
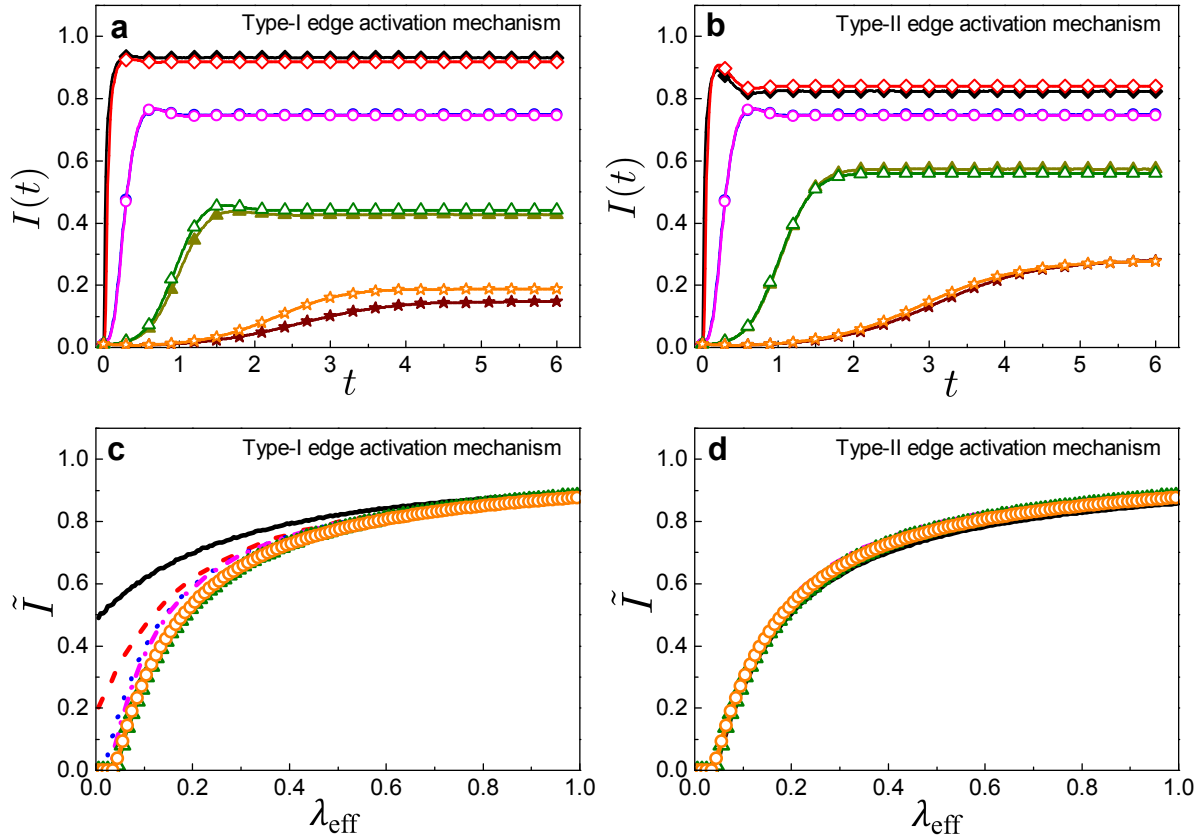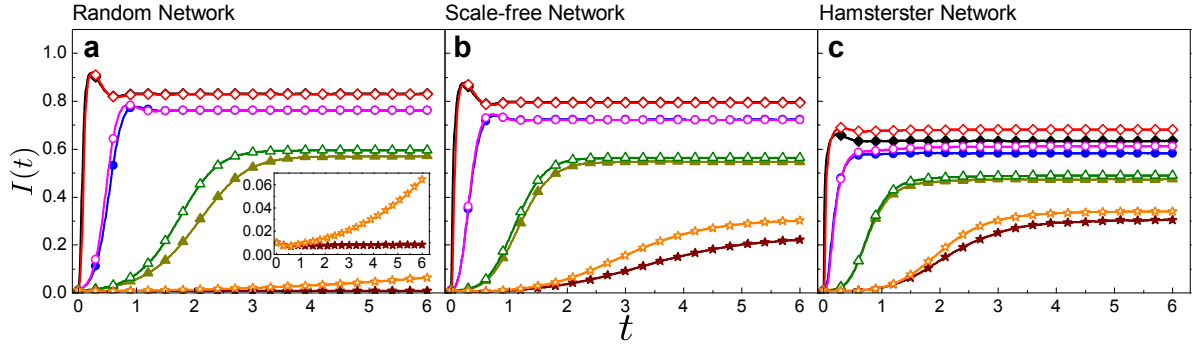
Supplementary Figure 7. Results on a scale-free network with strong heterogeneous degree distribution. **a,b** Comparison of time evolution between simulated and theoretical results for type-I and type-II activation mechanisms, respectively. The solid symbols represent the results of simulations which are averaged over 100 realizations. The open symbols denote the results of theoretical solutions. Diamonds, circles, triangles, and stars correspond to $\alpha_{\mathrm{I}} = 0.5, 1, 2, 4$, respectively. Other parameters are $\beta_{\mathrm{I}} = 1$, $\alpha_{\mathrm{R}} = 2$, and $\beta_{\mathrm{R}} = 0.5$. **c,d** Approximate equivalence between non-Markovian and Markovian processes with type-I and type-II activation mechanism, respectively. Solid, dashed, dotted, and dot-dashed curves, respectively, represent the results for $\alpha_{\mathrm{R}} = 0.5, 1, 2, 4$. Triangles and circles correspond to results from the Markovian process and analytical solutions, respectively. Other parameters are $\alpha_{\mathrm{I}} = 1$ and $\beta_{\mathrm{R}} = 0.5$.

SUPPLEMENTARY NOTE 9.   SPECIAL CASE III: NON-MARKOVIAN SPREADING ON NETWORKS WITH TYPE-III EDGE ACTIVATION MECHANISM

Besides the two edge activation mechanisms in the main text, other types of edge activation mechanisms exist. For example, rule #2 in Ref. [26] prescribes that the age of an active link is solely determined by the age of the infected node [27], which is similar but not totally identical to type-II edge activation treated in the main text. For convenience, we call this rule as type-III edge activation mechanism.

Because of the absence of any temporal correlation on active edges in type-III activation, the evolution equations are similar to those for type-II edge activation [Supplementary

Supplementary Figure 8. Comparison of time evolution for type-III activation mechanism. The three panels from left to right are for random, scale-free, and Hamsterster networks, respectively. In all panels, the solid symbols represent the results of simulations which are averaged over 100 realizations for random and scale-free networks, and over 400 realizations for the Hamsterster network obtained from Eqs. (7-9) in the main text and Supplementary Eq. (159). The open symbols represent the results of theoretical solutions. Diamonds, circles, triangles, and stars correspond to $\alpha_{\rm I} = 0.5, 1, 2, 4$, respectively. The random and scale-free networks have size $N = 10^4$ and mean degree $\langle k \rangle \approx 10$, and the Hamsterster network has $N = 2426$ and $\langle k \rangle \approx 13.7$. The inset in panel **a** shows the extinction process with $\alpha_{\rm I} = 4$. Other parameters are $\beta_{\rm I} = 1$, $\alpha_{\rm R} = 2$, and $\beta_{\rm R} = 0.5$.
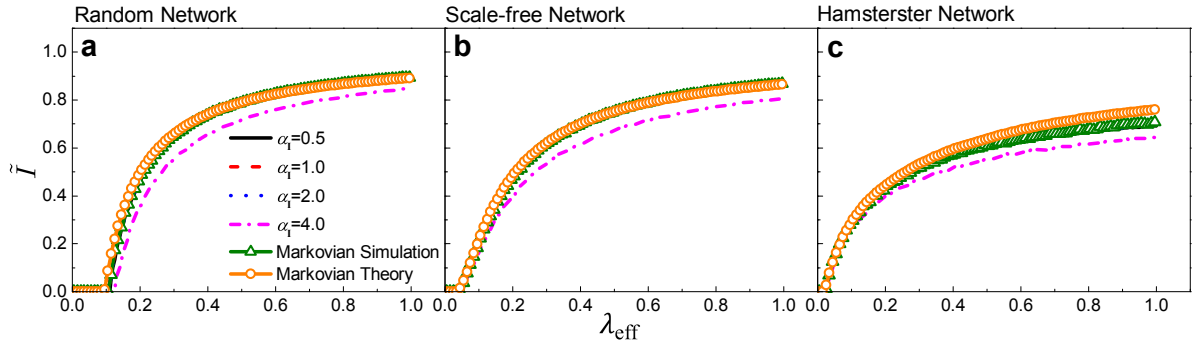
Supplementary Figure 9. Demonstration of equivalence with type-III edge activation mechanism. Comparison of stationary infected density between non-Markovian and Markovian processes. **a-c** Results from random, scale-free, and Hamsterster networks, respectively. Solid, dashed, dotted, and dot-dashed curves, respectively, represent the results for $\alpha_{\rm I} = 0.5, 1, 2, 4$. Triangles and circles represent simulation results from the Markovian process and the corresponding analytical solutions, respectively. Other parameters are $\alpha_{\rm R} = 2$ and $\beta_{\rm R} = 0.5$.

Eqs. (58) - (62)]. The only difference between these two activation mechanisms is the probability density function $\Phi_{i \leftarrow j}(\tau; t)$ in Supplementary Eq. (62). For type-III, $\Phi_{i \leftarrow j}(\tau; t)$ can be written as

$$\Phi_{i \leftarrow j}(\tau; t) = \int_0^t \omega_{\rm inf}(\tau') I_i(\tau', t) d\tau'. \tag{159}$$

24
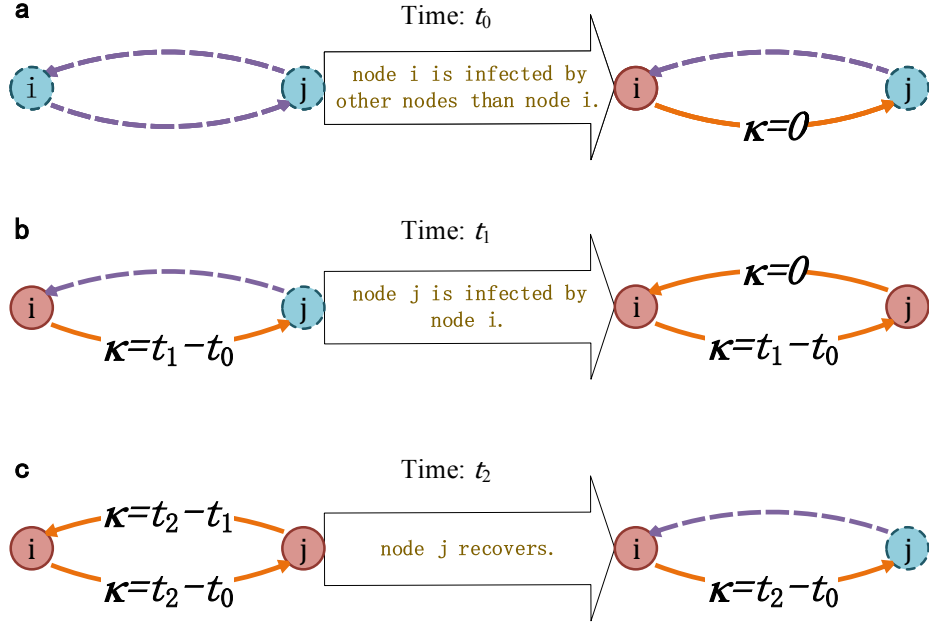
Supplementary Figure 10. An illustration of the growth of infection rate with type-III edge activation mechanism. The values of the relevant parameters are $\alpha_I = 4.0$ and $\beta_I = 1.0$, where the infection rate of an active age grows rapidly with time. **a** At $t_0 = 0$, node i is infected, and the active age is zero, so the infection rate is $\omega_{\text{inf}}(0) = 0$. **b** At $t_1 = 1$, the active edge transmits disease and node j moves into the infected state, but the age of the active edge from node i to node j remains unchanged. In this case, the infection rate is $\omega_{\text{inf}}(1) = 4$. **c** At time $t_2 = 2$, node j has recovered but node i is still in the infected state. The age of the active age is two. In this case, the infection rate is relatively large: $\omega_{\text{inf}}(2) = 32$. As a result, node i will make node j infected again in a short time.

Equations (63)-(68) suggest an equivalence between SIS dynamics with type-II activation and Markovian SIS dynamics, the effective infection rate can be obtained as

$$\lambda_{\text{eff}} \equiv \int_0^{+\infty} \eta(\tau)\Psi_{\text{rec}}(\tau)d\tau. \tag{160}$$

We can then conclude that SIS dynamics with type-III activation is equivalent to Markovian SIS dynamics with the effective infection rate given by

$$\lambda_{\text{eff}} \equiv \int_0^{+\infty} \omega_{\text{inf}}(\tau)\Psi_{\text{rec}}(\tau)d\tau. \tag{161}$$

To verify the above analysis, we simulate the dynamical processes and compare results with theoretical predictions. Supplementary Fig. 8 shows the time evolution of the infected density of the entire network for three different types of networks. We see that the mean-field predictions agree well with those of non-Markovian type of SIS spreading dynamics. We also find that a smaller value of α_I results in a larger scale outbreak on the networks, which is consistent with the cases of type-I and type-II edge activation mechanisms.

We further test the equivalence between non-Markovian and Markovian spreading process with type-III activation mechanism. Representative results are shown in Supplementary Fig. 9. It can be seen that, regardless of the network structure, the stationary infected density for $\alpha_I = 0.5, 1.0, 2.0$ agrees well with results from the simulation of Markovian process and from the analytical solution of the Markovian dynamics from Eq. (24) or Eq. (27) in the main text. However, the curve for $\alpha_I = 4$ deviates markedly from the case of Markovian dynamics. To explain this phenomenon, we note that the infection rate is

$$\omega_{\text{inf}}(\kappa) = \frac{\alpha_I}{\beta_I}(\frac{\kappa}{\beta_I})^{\alpha_I-1}, \tag{162}$$

while the infection times follow a Weibullean distribution:

$$\psi_{\text{inf}}(\kappa) = \frac{\alpha_I}{\beta_I}(\frac{\kappa}{\beta_I})^{\alpha_I-1}e^{-(\frac{\kappa}{\beta_I})^{\alpha_I}}. \tag{163}$$

For $\alpha_I > 1$, $\omega_{\text{inf}}(\kappa)$ increases with κ. A greater value of α_I results in faster growth of $\omega_{\text{inf}}(\kappa)$ with κ. Since the age of an active edge cannot be zero after it transmits the disease, the value of the infection rate $\omega_{\text{inf}}(\kappa)$ will keep increasing until the corresponding infected node recovers. Supplementary Fig. 10 shows an example of how the infection rate of an active edge increases sharply with κ. The persistent enhancement effect of infection rate with time makes it harder for the mean-field theory to capture the dynamical correlation on the active edge, generating deviations between the simulation result for $\alpha_I = 4$ from the mean-field prediction.

SUPPLEMENTARY REFERENCES

[1] Liptaj, A. Higher order derivatives of the inverse function (2007).

[2] Van Mieghem, P. *Performance Analysis of Communications Networks and Systems* (Cambridge University Press, 2009).

[3] Anderson, R. M. & May, R. M. *Infectious Diseases of Humans: Dynamics and Control* (Oxford University Press, 1992).

[4] Pastor-Satorras, R. & Vespignani, A. Epidemic spreading in scale-free networks. *Phys. Rev. Lett.* **86**, 3200 (2001).

[5] Van Mieghem, P., Omic, J. & Kooij, R. Virus spread in networks. *IEEE/ACM Trans. Network. (TON)* **17**, 1–14 (2009).

[6] Van Mieghem, P. The n-intertwined SIS epidemic network model. *Computing* **93**, 147–169 (2011).

[7] Rand, D. Correlation equations and pair approximations for spatial ecologies. *Chapter 4 in Advanced Ecological Theory: Principles and Applications* **100** (1999).

[8] Keeling, M. J. The effects of local spatial structure on epidemiological invasions. *Proc. R. Soc. Lond. B* **266**, 859–867 (1999).

[9] Keeling, M. & Rand, D. Spatial correlations and local fluctuations in host-parasite models. *in From Finite to Infinite Dimensional Dynamical Systems* 5–57 (2001).

[10] Georgiou, N., Kiss, I. Z. & Scalas, E. Solvable non-Markovian dynamic network. *Phys. Rev. E* **92**, 042801 (2015).

[11] Kiss, I. Z., Röst, G. & Vizi, Z. Generalization of pairwise models to non-Markovian epidemics on networks. *Phys. Rev. Lett.* **115**, 078701 (2015).

[12] Sherborne, N., Miller, J. C., Blyuss, K. B. & Kiss, I. Z. Mean-field models for non-Markovian epidemics on networks. *J. Math. Biol.* **76**, 755–778 (2018).

[13] Eames, K. T. & Keeling, M. J. Modeling dynamic and network heterogeneities in the spread of sexually transmitted diseases. *Proc. Nat. Acad. Sci. (USA)* **99**, 13330–13335 (2002).

[14] Gleeson, J. P. High-accuracy approximation of binary-state dynamics on networks. *Phys. Rev. Lett.* **107**, 068701 (2011).

[15] Vazquez, A., Racz, B., Lukacs, A. & Barabasi, A.-L. Impact of non-Poissonian activity patterns on spreading processes. *Phys. Rev. Lett.* **98**, 158702 (2007).

[16] Min, B., Goh, K.-I. & Vazquez, A. Spreading dynamics following bursty human activity patterns. *Phys. Rev. E* **83**, 036102 (2011).

[17] Iribarren, J. L. & Moro, E. Impact of human activity patterns on the dynamics of information diffusion. *Phys. Rev. Lett.* **103**, 038702 (2009).

[18] Iribarren, J. L. & Moro, E. Branching dynamics of viral information spreading. *Phys. Rev. E* **84**, 046116 (2011).

[19] Fernández-Gracia, J., Eguíluz, V. M. & San Miguel, M. Update rules and interevent time distributions: Slow ordering versus no ordering in the voter model. *Phys. Rev. E* **84**, 015103 (2011).

[20] Watts, D. J. & Strogatz, S. H. Collective dynamics of small-world networks. *Nature* **393**, 440 (1998).

[21] Barthélemy, M., Barrat, A., Pastor-Satorras, R. & Vespignani, A. Velocity and hierarchical spread of epidemic outbreaks in scale-free networks. *Phys. Rev. Lett.* **92**, 178701 (2004).

[22] Pastor-Satorras, R. & Vespignani, A. Epidemic spreading in scale-free networks. *Phys. Rev. Lett.* **86**, 3200 (2001).

[23] Boguá, M., Pastor-Satorras, R. & Vespignani, A. Epidemic spreading in complex networks with degree correlations. In *Statistical mechanics of complex networks*, 127–147 (Springer, 2003).

[24] Onnela, J.-P. *et al.* Structure and tie strengths in mobile communication networks. *Proc. Nat. Acad. Sci. (USA)* **104**, 7332–7336 (2007).

[25] Park, Y., Moore, C. & Bader, J. S. Dynamic networks from hierarchical Bayesian graph clustering. *PloS one* **5**, e8118 (2010).

[26] Boguná, M., Lafuerza, L. F., Toral, R. & Serrano, M. Á. Simulating non-Markovian stochastic processes. *Phys. Rev. E* **90**, 042108 (2014).

[27] Van Mieghem, P. & van de Bovenkamp, R. Non-Markovian infection spread dramatically alters the susceptible-infected-susceptible epidemic threshold in networks. *Phys. Rev. Lett.* **110**, 108701 (2013).

[28] Catanzaro, M., Boguná, M. & Pastor-Satorras, R. Generation of uncorrelated random scale-free networks. *Phys. Rev. E* **71**, 027103 (2005).